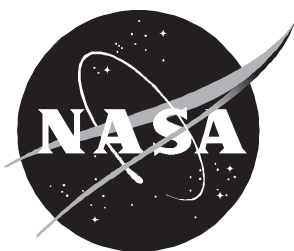




Finite Element Method for Eigenvalue Problems in Electromagnetics

C. J. Reddy, Manohar D. Deshpande, C. R. Cockrell, and Fred B. Beck



Finite Element Method for Eigenvalue Problems in Electromagnetics

C. J. Reddy

Langley Research Center • Hampton, Virginia

Manohar D. Deshpande

ViGYAN, Inc. • Hampton, Virginia

C. R. Cockrell and Fred B. Beck

Langley Research Center • Hampton, Virginia

This publication is available from the following sources:

NASA Center for Aerospace Information
800 Elkridge Landing Road
Linthicum Heights, MD 21090-2934
(301) 621-0390

National Technical Information Service (NTIS)
5285 Port Royal Road
Springfield, VA 22161-2171
(703) 487-4650

Contents

Symbols	vii
Abstract	1
1. Introduction	1
2. Two-Dimensional Problems	2
2.1. Homogeneous Waveguides—Scalar Formulation	2
2.1.1. Formulation	2
2.1.2. Discretization	2
2.1.3. Field Computation From Scalar Potential	4
2.1.4. Numerical Examples	4
2.1.5. Summary	8
2.2. Inhomogeneous Waveguides—Vector Formulation	8
2.2.1. Solution of Homogeneous Waveguide Problem With Two-Component Transverse Vector Fields	10
2.2.1.1. Formulation	10
2.2.1.2. Discretization	10
2.2.1.3. Finite element formulation	11
2.2.1.4. Finite element matrices	12
2.2.1.5. Numerical examples	12
2.2.2. Inhomogeneous Waveguide Problems Using Three-Component Vector Fields	12
2.2.2.1. Formulation	13
2.2.2.2. Discretization	13
2.2.2.3. Finite element formulation	13
2.2.2.4. Finite element matrices	14
2.2.2.5. Numerical examples	14
2.2.3. Wave-Number Determination for Given Propagation Constant	15
2.2.3.1. Formulation	15
2.2.3.2. Discretization	16
2.2.3.3. Finite element formulation	16
2.2.3.4. Finite element matrices	17
2.2.3.5. Numerical example	17
2.2.4. Dispersion Characteristics of Waveguides	17
2.2.4.1. Formulation	17
2.2.4.2. Discretization	17
2.2.4.3. Finite element formulation	18
2.2.4.4. Finite element matrices	18
2.2.4.5. Numerical examples	19
2.2.5. Summary	19
3. Three-Dimensional Problems	19
3.1. Eigenvalues of Three-Dimensional Cavity—Vector Formulation	19
3.1.1. Formulation	20
3.1.2. Discretization	21
3.1.3. Finite Element Formulation	22
3.1.4. Finite Element Matrices	22

3.1.5. Numerical Examples	23
3.1.6. Summary	24
4. Concluding Remarks	24
Appendix	26
References	27

Tables

Table 1. Cutoff Wave Numbers for Rectangular Waveguide	5
Table 2. Cutoff Wave Numbers for Circular Waveguide	5
Table 3. Cutoff Wave Numbers for Coaxial Line With $r_2/r_1 = 4$	8
Table 4. Cutoff Wave Numbers for Rectangular Waveguide	12
Table 5. Cutoff Wave Numbers for Circular Waveguide	13
Table 6. Cutoff Wave Numbers for Rectangular Waveguide	14
Table 7. Cutoff Wave Numbers for Circular Waveguide	14
Table 8. Wave Numbers for LSM Modes of Square Waveguide With $\beta = 10$	17
Table 9. Dispersion Characteristics of Partially Filled Rectangular Waveguide of Figure 12	19
Table 10. Dispersion Characteristics of Partially Filled Rectangular Waveguide of Figure 13	20
Table 11. Formation of Edges of Tetrahedral Element	21
Table 12. Eigenvalues of Air-Filled Rectangular Cavity	23
Table 13. Eigenvalues of Half-Filled Rectangular Cavity	24
Table 14. Eigenvalues of Air-Filled Circular Cylindrical Cavity	24
Table 15. Eigenvalues of Spherical Cavity With Radius of 1 cm	24

Figures

Figure 1. Geometry of problem.	2
Figure 2. Single triangular element.	2
Figure 3. Flowchart for FEM solution.	4
Figure 4. Geometry of rectangular waveguide.	5
Figure 5. Electric field distribution of some modes for rectangular waveguide.	6
Figure 6. Cross section of circular waveguide.	6
Figure 7. Electric field distribution of some modes for circular waveguide.	7
Figure 8. Cross section of coaxial line.	8
Figure 9. Electric field distribution of some modes for coaxial line.	9
Figure 10. Configuration of tangential edge elements.	11
Figure 11. Partially filled square waveguide.	17
Figure 12. Partially filled rectangular waveguide with $b_r/a_r = 0.45$, $d/b_r = 0.5$, and $\varepsilon_r = 2.45$	19
Figure 13. Partially filled waveguide with $b_r/a_r = 0.45$ and $\varepsilon_r = 2.45$	19
Figure 14. First-order tetrahedral element.	21
Figure 15. Air-filled rectangular cavity. Size: 1 by 0.5 by 0.75 cm.	23
Figure 16. Half-filled rectangular cavity with dielectric material $\varepsilon_r = 2.0$ and filled from $z = 0.5$ to 1 cm. Size: 1 by 0.1 by 1 cm.	23
Figure 17. Air-filled circular cylindrical cavity. Dimensions are in centimeters.	24

Symbols

A, B	generic vectors used in vector identities
A	area of triangle
$A_m, A_{xm}, A_{ym}, A_{zm}$	coefficients defined by equations (57), (164), (167), and (170), $m = 1, 2, \dots, 6$
a_i, b_i, c_i	coefficients defined by equations (16), (17), and (18), $i = 1, 2, 3$
a_r, b_r	dimensions of rectangular waveguide
$a_{tm}, b_{tm}, c_{tm}, d_{tm}$	coefficients of α_{tm} as defined in equation (162), $m = 1, 2, 3, 4$
$B_m, B_{xm}, B_{ym}, B_{zm}$	coefficients defined by equations (58), (165), (168), and (171), $m = 1, 2, \dots, 6$
$C_m, C_{xm}, C_{ym}, C_{zm}$	coefficients defined by equations (59), (166), (169), and (172), $m = 1, 2, \dots, 6$
D_m	coefficient defined in equation (60)
dl	line integral
ds	surface integral
dv	volume integral
$d\Gamma$	boundary contour of waveguide
E	electric field, $E_x\hat{x} + E_y\hat{y} + E_z\hat{z}$
E_t	transverse electric field, $E_x\hat{x} + E_y\hat{y}$
E_x, E_y, E_z	components of vector E
e_m	unknown coefficient at edges of tetrahedral element, $m = 1, 2, \dots, 6$
e_{tm}	unknown coefficient at edges of triangular element, $m = 1, 2, 3$
e_{zi}	unknown coefficient of field at nodes of triangle as defined by equation (94), $i = 1, 2, 3$
FEM3D0, FEM3D1	computer codes for three-dimensional eigenvalue solvers
f	generic scalar used in vector identities
H	magnetic field, $H_x\hat{x} + H_y\hat{y} + H_z\hat{z}$
H_t	transverse magnetic field, $H_x\hat{x} + H_y\hat{y}$
H_x, H_y, H_z	components of vector H
HELM10	computer code for two-dimensional scalar eigenvalue solver
HELMVEC, HELMVEC1, HELMVEC2, HELMVEC3	computer codes for two-dimensional vector eigenvalue solvers
k_c	cutoff wave number
k_o	free-space wave number, $\frac{2\pi}{\lambda_o}$
L_m	length of edges for tetrahedral element, $m = 1, 2, 3, 4$
L_{tm}	length of edges for triangular element, $m = 1, 2, 3$

LSM	longitudinal section magnetic
\hat{n}	unit normal
PEC	perfect electric conductor
r	radius of circular waveguide
r_1	radius of inner conductor of coaxial line
r_2	radius of outer conductor of coaxial line
S , T	FEM global matrices
S _{el} , T _{el}	FEM element matrices
$S_{\text{el}(tt)}, S_{\text{el}(tz)},$ $S_{\text{el}(zt)}, S_{\text{el}(zz)}$	FEM element submatrices as defined in equations (112) and (139)
$S_{tt}, S_{tz}, S_{zt}, S_{zz}$	FEM global submatrices as defined in equations (119) and (135)
S_t, T_t	global matrices for transverse fields as defined in equation (92)
S_z, T_z	global matrices for longitudinal fields as defined in equation (92)
T	vector testing function, $T_x\hat{x} + T_y\hat{y} + T_z\hat{z}$
$T_{\text{el}(tt)}, T_{\text{el}(tz)},$ $T_{\text{el}(zt)}, T_{\text{el}(zz)}$	FEM element submatrices as defined in equations (112) and (129)
T _t	two-dimensional vector testing function, $T_x\hat{x} + T_y\hat{y}$
T _s	two-dimensional scalar testing function
$T_{tt}, T_{tz}, T_{zt}, T_{zz}$	FEM global submatrices as defined in equations (119) and (135)
T_x, T_y, T_z	components of vector T
TE	transverse electric
TM	transverse magnetic
\hat{t}_m	unit vector along edge of tetrahedral element, $m = 1, 2, \dots, 6$
\hat{t}_{tm}	unit vector along edge of triangular element, $m = 1, 2, 3$
V	volume of tetrahedron
W _m	edge basis function for tetrahedral elements, $m = 1, 2, \dots, 6$
W _{tm}	edge basis function for triangular elements, $m = 1, 2, 3$
X, Y, Z	rectangular coordinate axes
x, y, z	rectangular coordinates
$\hat{x}, \hat{y}, \hat{z}$	unit vectors along X-, Y-, and Z-axis, respectively
$\bar{x}_{\text{tet}}, \bar{y}_{\text{tet}}, \bar{z}_{\text{tet}}$	centroid of tetrahedral element
$\bar{x}_{\text{tri}}, \bar{y}_{\text{tri}}$	centroid of triangular element
Z_o^{TM}	characteristic impedance of TE mode
α_i	first-order shape function for triangular element defined by equation (15), $i = 1, 2, 3$

α_{tm}	first-order shape function for a tetrahedral element, $m = 1, 2, 3, 4$
β	waveguide propagation constant
Γ	waveguide cross-section area
Δ	integration over surface of triangular element
\blacktriangle	integration over volume of tetrahedral element
ε_r	relative permittivity
λ_o	free-space wavelength
μ_r	relative permeability
ψ	two-dimensional scalar potential function, TE or TM
ψ_i	unknown coefficients of ψ at nodes of triangular element, $i = 1, 2, 3$
∇	three-dimensional gradient operator in rectangular coordinates
∇_t	two-dimensional gradient operator in X - Y plane

Abstract

Finite element method (FEM) has been a very powerful tool to solve many complex problems in electromagnetics. The goal of the current research at the Langley Research Center is to develop a combined FEM/method of moments approach to three-dimensional scattering/radiation problem for objects with arbitrary shape and filled with complex materials. As a first step toward that goal, an exercise is taken to establish the power of FEM, through closed boundary problems. This paper demonstrates the development of FEM tools for two- and three-dimensional eigenvalue problems in electromagnetics. In section 2, both the scalar and vector finite elements have been used for various waveguide problems to demonstrate the flexibility of FEM. In section 3, vector finite element method has been extended to three-dimensional eigenvalue problems.

1. Introduction

The finite element method (FEM) has been widely used as an analysis and design tool in many engineering disciplines like structures and computational fluid mechanics. Though FEM has been applied to electromagnetic problems, it was mainly confined to electrical machines and magnetics (ref. 1). In the past 20 years there has been a great interest in application of this method to microwave components such as waveguides and antennas. But for many years, its use has been restricted because of the so-called spurious solutions in vector finite elements (ref. 2). Very recently, the "edge elements" have been employed successfully for vector formulations without resulting in "spurious solutions." In the recent past, use of these edge elements in FEM has revived an interest in applying FEM to microwave engineering problems (ref. 3). This in combination with the advances in computer hardware and software helped to make FEM an attractive tool for electromagnetics. Also, there are a variety of commercial geometrical modelling tools to accurately model any three-dimensional geometry and to generate the required mesh with any kind of elements such as triangles and tetrahedrals (refs. 4 and 5).

In this paper, the FEM tools for analyzing eigenvalue problems in electromagnetics have been described. This paper is divided into two parts: section 2 deals with the two-dimensional problems; section 3, with the three-dimensional problems. Throughout this paper triangular elements are used for modelling two-dimensional problems and tetrahedrals are used to model the three-dimensional problems.

In section 2.1, a scalar FEM formulation is used for two-dimensional arbitrarily shaped waveguides. Triangular elements with nodal basis functions are

used to formulate the FEM matrices. The eigenvalues for different types of waveguides are obtained and the field intensity plots are presented for various waveguide modes.

In section 2.2, a vector FEM is introduced with two-dimensional edge elements for analyzing inhomogeneous waveguides. For the sake of clarity in formulation, section 2.2 is divided into four sections. Section 2.2.1 gives the solution of homogeneous waveguide problem with two-component transverse vector fields. Section 2.2.2 gives the calculation of eigenvalues for inhomogeneous waveguides using the three-component vector fields. Combination of edge and nodal basis functions have been used for transverse and longitudinal field components, respectively. Sections 2.2.3 and 2.2.4 extend the formulation in section 2.2.2 to determine either the wave number or the propagation constant for inhomogeneously filled waveguides when one of them is specified.

In section 3.1, formulation for three-dimensional vector FEM is described. Edge basis functions for tetrahedral elements are introduced to formulate finite element matrices for three-dimensional cavities filled with inhomogeneous material.

In sections 2.1, 2.2, and 3.1, numerical examples are presented to show the validity of the analysis and the computer programs developed. For all the examples, FEM results in good accuracy. All the numerical examples have been checked for numerical convergence. By virtue of FEM, the computer codes presented in this paper can handle any arbitrarily shaped geometries filled with inhomogeneous materials, unless otherwise mentioned.

2. Two-Dimensional Problems

2.1. Homogeneous Waveguides—Scalar Formulation

This section deals with the solution of two-dimensional waveguide problems with closed boundaries using the Galerkin finite element method. The wave equation is solved for a generalized problem with nodal-based first-order triangular elements (ref. 1). Finite element matrices are derived and a computer program to calculate the eigenvalues and electric field distributions is presented.

2.1.1. Formulation

The scalar potential function ψ satisfies the Helmholtz equation with wave number k_c

$$\nabla_t^2 \psi + k_c^2 \psi = 0 \quad (1)$$

within and on the boundary $d\Gamma$ indicated in figure 1. This is the “strong” form of the scalar Helmholtz equation. In the strong form, the unknown appears within a second-order differential operator. To make the equation suitable for a numerical solution, it can be converted into the “weak” form by multiplying both sides with a testing function T_s and integrating over the surface Γ ; that is,

$$\iint_{\Gamma} [T_s (\nabla_t^2 \psi) + k_c^2 T_s \psi] ds = 0 \quad (2)$$

The first term in equation (2) can be written as

$$\iint_{\Gamma} T_s (\nabla_t^2 \psi) ds = \iint_{\Gamma} T_s (\nabla_t \cdot \nabla_t \psi) ds \quad (3)$$

The following vector identities can be used to modify equation (3):

$$\nabla_t \cdot [T_s (\nabla_t \psi)] = \nabla_t T_s \cdot \nabla_t \psi + T_s (\nabla_t \cdot \nabla_s \psi) \quad (4)$$

and

$$\iint_{\Gamma} \nabla_t \cdot \nabla_t \psi ds = \int_{d\Gamma} \nabla_t \psi \cdot \hat{n} dl \quad (5)$$

where \hat{n} is the unit normal along the boundary $d\Gamma$. Equation (2) can now be written as

$$\iint_{\Gamma} (\nabla_t T_s \cdot \nabla_t \psi) ds - k_c^2 \iint_{\Gamma} T_s \psi ds = \int_{d\Gamma} T_s \frac{\partial \psi}{\partial n} dl \quad (6)$$

where $\partial \psi / \partial n$ is the normal derivative of ψ along the boundary $d\Gamma$. The term on the right-hand side vanishes as T_s vanishes on the PEC boundary for the TM case and $\partial \psi / \partial n$ vanishes at the boundary for the TE case. Hence equation (6) can be written as

$$\iint_{\Gamma} (\nabla_t T_s \cdot \nabla_t \psi) ds = k_c^2 \iint_{\Gamma} T_s \psi ds \quad (7)$$

2.1.2. Discretization

The problem region is discretized with the first-order triangular elements. Within the triangular element given in figure 2, ψ is adequately approximated by the expression (ref. 1)

$$\psi = a + bx + cy \quad (8)$$

The solution is piecewise planar but continuous everywhere. At the vertices 1, 2, and 3, the potential can be expressed as

$$\psi_1 = a + bx_1 + cy_1 \quad (9)$$

$$\psi_2 = a + bx_2 + cy_2 \quad (10)$$

$$\psi_3 = a + bx_3 + cy_3 \quad (11)$$

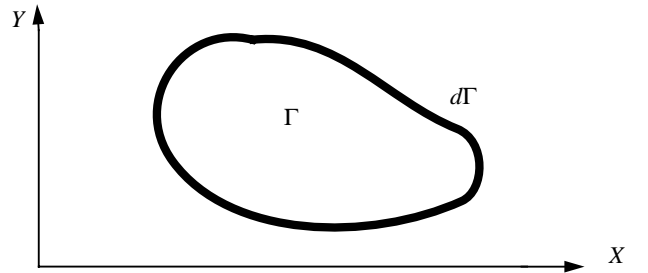


Figure 1. Geometry of problem.

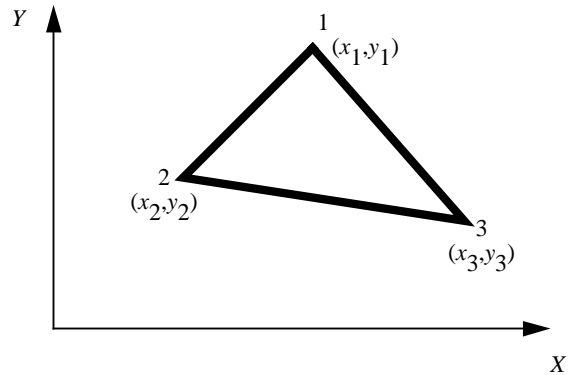


Figure 2. Single triangular element.

From equations (9), (10), and (11), the coefficients a , b , and c are evaluated as

$$\begin{bmatrix} a \\ b \\ c \end{bmatrix} = \begin{bmatrix} 1 & x_1 & y_1 \\ 1 & x_2 & y_2 \\ 1 & x_3 & y_3 \end{bmatrix}^{-1} \begin{bmatrix} \psi_1 \\ \psi_2 \\ \psi_3 \end{bmatrix} \quad (12)$$

Hence, equation (8) can be rewritten by substituting for a , b , and c

$$\psi = \begin{bmatrix} 1 & x & y \end{bmatrix} \begin{bmatrix} a \\ b \\ c \end{bmatrix} = \begin{bmatrix} 1 & x & y \end{bmatrix} \begin{bmatrix} 1 & x_1 & y_1 \\ 1 & x_2 & y_2 \\ 1 & x_3 & y_3 \end{bmatrix}^{-1} \begin{bmatrix} \psi_1 \\ \psi_2 \\ \psi_3 \end{bmatrix} \quad (13)$$

Equation (13) can be written as

$$\psi = \sum_{i=1}^3 \psi_i \alpha_i(x, y) \quad (14)$$

where $\alpha_i(x, y)$ is given by

$$\alpha_i(x, y) = \frac{1}{2A}(a_i + b_i x + c_i y) \quad (i = 1, 2, 3) \quad (15)$$

and a_i , b_i , and c_i are given by

$$a_i = x_j y_k - x_k y_j \quad (16)$$

$$b_i = y_j - y_k \quad (17)$$

$$c_i = x_k - x_j \quad (18)$$

where i , j , and k are cyclical; that is ($i = 1, j = 2, k = 3$), ($i = 2, j = 3, k = 1$) and ($i = 3, j = 1, k = 2$), and A is given by

$$A = \frac{1}{2} \begin{vmatrix} 1 & x_1 & y_1 \\ 1 & x_2 & y_2 \\ 1 & x_3 & y_3 \end{vmatrix} \quad (19)$$

Using the testing function (as per Galerkin's technique (ref. 1)),

$$T_s = \alpha_j(x, y) \quad (j = 1, 2, 3) \quad (20)$$

and the element representation in equation (14), the left-hand side of equation (7) can be evaluated over a single element as

$$\begin{aligned} & \iint_{\Delta} (\nabla T_s \cdot \nabla \psi) dx dy \\ &= \sum_{i=1}^3 \psi_i \iint_{\Delta} (\nabla \alpha_i \cdot \nabla \alpha_j) dx dy \quad (j = 1, 2, 3) \end{aligned} \quad (21)$$

and the right-hand side as

$$\iint_{\Delta} T_s \psi dx dy = \sum_{i=1}^3 \psi_i \iint_{\Delta} \alpha_i \alpha_j dx dy \quad (j = 1, 2, 3) \quad (22)$$

Hence for each element, equation (7) becomes

$$\begin{aligned} & \sum_{i=1}^3 \psi_i \iint_{\Delta} (\nabla \alpha_i \cdot \nabla \alpha_j) dx dy \\ &= k_c^2 \sum_{i=1}^3 \psi_i \iint_{\Delta} \alpha_i \alpha_j dx dy \quad (j = 1, 2, 3) \end{aligned} \quad (23)$$

And this can be written in a matrix form as

$$[\mathbf{S}_{el}][\psi] = k_c^2 [\mathbf{T}_{el}][\psi] \quad (24)$$

where

$$[\mathbf{S}_{el}] = \iint_{\Delta} (\nabla \alpha_i \cdot \nabla \alpha_j) dx dy \quad (25)$$

$$[\mathbf{T}_{el}] = \iint_{\Delta} (\alpha_i \alpha_j) dx dy \quad (26)$$

$$\nabla \alpha_i = \frac{\partial \alpha_i}{\partial x} \hat{x} + \frac{\partial \alpha_i}{\partial y} \hat{y} \quad (27)$$

From equation (15), $\nabla \alpha_i$ can be written as

$$\nabla \alpha_i = \frac{1}{2A}(b_i \hat{x} + c_i \hat{y}) \quad (28)$$

and hence,

$$[\nabla \alpha_i \cdot \nabla \alpha_j] = \begin{bmatrix} \nabla \alpha_1 \cdot \nabla \alpha_1 & \nabla \alpha_1 \cdot \nabla \alpha_2 & \nabla \alpha_1 \cdot \nabla \alpha_3 \\ \nabla \alpha_2 \cdot \nabla \alpha_1 & \nabla \alpha_2 \cdot \nabla \alpha_2 & \nabla \alpha_2 \cdot \nabla \alpha_3 \\ \nabla \alpha_3 \cdot \nabla \alpha_1 & \nabla \alpha_3 \cdot \nabla \alpha_2 & \nabla \alpha_3 \cdot \nabla \alpha_3 \end{bmatrix} \quad (29)$$

Substituting equation (28) into equation (29) gives

$$[\nabla \alpha_i \cdot \nabla \alpha_j] = \frac{1}{4A^2} \begin{bmatrix} b_1^2 + c_1^2 & b_1 b_2 + c_1 c_2 & b_1 b_3 + c_1 c_3 \\ b_2 b_1 + c_2 c_1 & b_2^2 + c_2^2 & b_2 b_3 + c_2 c_3 \\ b_3 b_1 + c_3 c_1 & b_3 b_2 + c_3 c_2 & b_3^2 + c_3^2 \end{bmatrix} \quad (30)$$

The matrix $[\mathbf{S}_{el}]$ can be evaluated by using equation (30) to obtain

$$[\mathbf{S}_{el}] = \left[\iint_{\Delta} (\nabla \alpha_i \cdot \nabla \alpha_j) dx dy \right] = A [\nabla \alpha_i \cdot \nabla \alpha_j] \quad (31)$$

$$[\mathbf{T}_{el}] = \left[\iint_{\Delta} \alpha_i \alpha_j dx dy \right] \quad (32)$$

The matrix $[\mathbf{T}_{el}]$ has been evaluated by Silvester (ref. 6) and is given in a simple form as

$$[\mathbf{T}_{el}] = \frac{A}{12} \begin{bmatrix} 2 & 1 & 1 \\ 1 & 2 & 1 \\ 1 & 1 & 2 \end{bmatrix} \quad (33)$$

The matrices $[\mathbf{S}_{el}]$ and $[\mathbf{T}_{el}]$ are evaluated for each element and are assembled over the entire region according to the global node numbering to obtain a global matrix equation (ref. 1) as follows:

$$[\mathbf{S}][\psi] = k_c^2 [\mathbf{T}][\psi] \quad (34)$$

This results in matrices of the order $n \times n$ where n is total number of nodes. With equations (30), (31), and (33), the eigenvalue equation (eq. (34)) is solved for k_c^2 by the standard eigenvalue solvers from the EISPACK library (refs. 7 and 8). The cutoff wave numbers are then given by $\sqrt{k_c^2}$.

2.1.3. Field Computation From Scalar Potential

Once the scalar potential is calculated at every node, the electric field can be calculated for both the TE and TM modes by the following formulation. The scalar potential at any point (x, y) inside a triangular element is given by

$$\psi = \sum_{i=1}^3 \psi_i \alpha_i(x, y) \quad (35)$$

These scalar potentials can be differentiated with respect to x and y to obtain the following expressions:

$$\frac{\partial \psi}{\partial x} = \frac{1}{2A} \sum_{i=1}^3 \psi_i b_i \quad (36)$$

$$\frac{\partial \psi}{\partial y} = \frac{1}{2A} \sum_{i=1}^3 \psi_i c_i \quad (37)$$

For the TE modes, the transverse electric field components E_x and E_y inside an element are given by

$$E_x = -\frac{\partial \psi}{\partial y} \quad (38)$$

$$E_y = \frac{\partial \psi}{\partial x} \quad (39)$$

When obtaining the scalar potential for the TM modes, the scalar potential is set to zero on PEC

walls of the waveguide to satisfy the Dirichlet boundary conditions for the longitudinal electric field component. A very simple way of implementing this is to ignore the nodes on PEC while forming finite element matrices. This will result in lower order matrices for the TM case than those for the TE case. Once the scalar potential is obtained, the transverse electric fields for the TM modes are given by

$$E_x = -Z_o^{\text{TM}} \frac{\partial \psi}{\partial x} \quad (40)$$

$$E_y = -Z_o^{\text{TM}} \frac{\partial \psi}{\partial y} \quad (41)$$

where Z_o^{TM} is the characteristic wave impedance for the TM mode.

2.1.4. Numerical Examples

A computer code HELM10 was written to implement the formulation presented in section 2.1. The flowchart for the implementation of the FEM solution is given in figure 3. Numerical examples for the rectangular waveguide, the circular waveguide, and the coaxial line are given as follows:

Rectangular waveguide: The cutoff wave numbers k_c of a rectangular waveguide calculated by using HELM10 are presented in table 1 along with analytical results from reference 9. The geometry of the rectangular waveguide ($a_r/b_r = 2$) is shown in figure 4. The numerical results presented are achieved with 400 triangular elements over the cross section of the waveguide. The eigenvectors for some of the modes have been calculated and the electric fields of the corresponding modes are plotted in figure 5.

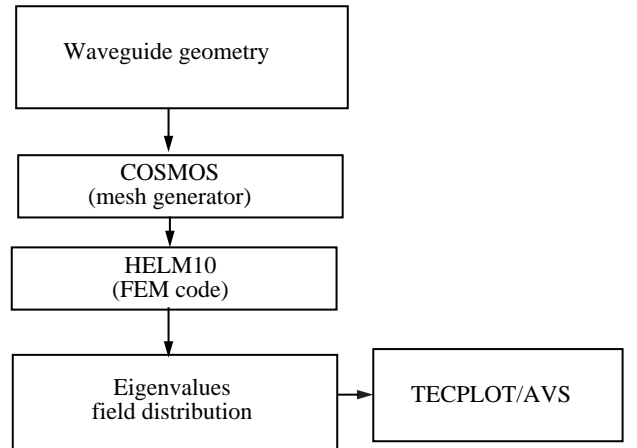


Figure 3. Flowchart for FEM solution.

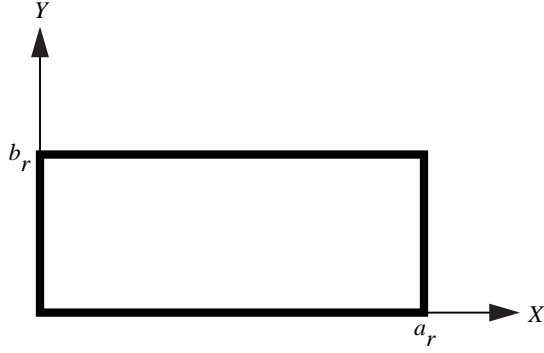


Figure 4. Geometry of rectangular waveguide.

Circular waveguide: The cutoff wave numbers for a circular waveguide of unit radius were calculated with HELM10 and compared with analytically avail-

able data from reference 9. (See table 2.) A cross section of the circular waveguide is shown in figure 6. Two hundred triangular elements have been used to model the geometry. The eigenvectors of selected modes have been calculated and the electric fields of these modes are plotted in figure 7.

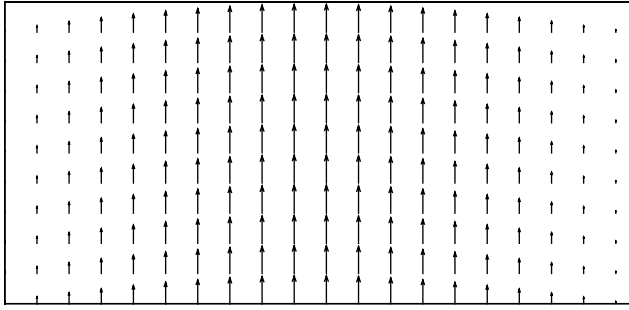
Coaxial line: The cross section of the coaxial line is shown in figure 8. The HELM10 program is used to calculate the cutoff wave numbers and corresponding electric field strength of higher order TE and TM modes. A triangular mesh with 340 elements has been used to model the geometry. Table 3 presents the cutoff wave numbers computed for $r_2/r_1 = 4$ by HELM10 and the analytically available cutoff wave numbers in the literature (ref. 10). For TM modes the potential on the inner and outer conductors is set to zero. The transverse electric field components are calculated and plotted in figure 9.

Table 1. Cutoff Wave Numbers for Rectangular Waveguide

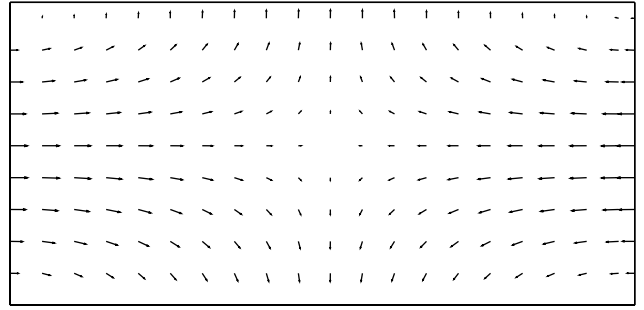
TE	TM	$k_c a_r$	
		Analytical (ref. 9)	HELM10
10		3.142	3.144
20		6.285	6.308
01		6.285	6.308
11	11	7.027	7.027
12	12	12.958	13.201
21	21	8.889	8.993

Table 2. Cutoff Wave Numbers for Circular Waveguide

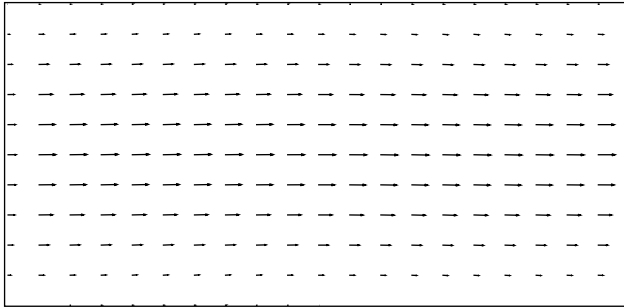
Mode	$k_c r$	
	Analytical (ref. 9)	HELM10
TE ₀₁	3.832	3.858
TE ₁₁	1.841	1.843
TE ₁₂	5.331	5.379
TE ₂₁	3.054	3.068
TE ₂₂	6.706	6.688
TM ₀₁	2.405	2.413
TM ₁₁	3.832	3.854
TM ₁₂	7.016	7.136
TM ₂₁	5.135	5.210
TM ₂₂	8.417	8.668



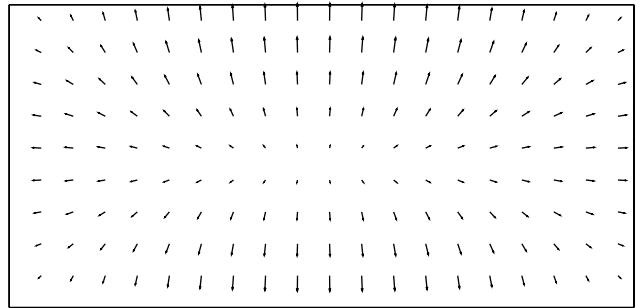
(a) TE_{10} mode.



(b) TE_{11} mode.



(c) TE_{01} mode.



(d) TM_{11} mode.

Figure 5. Electric field distribution of some modes for rectangular waveguide.

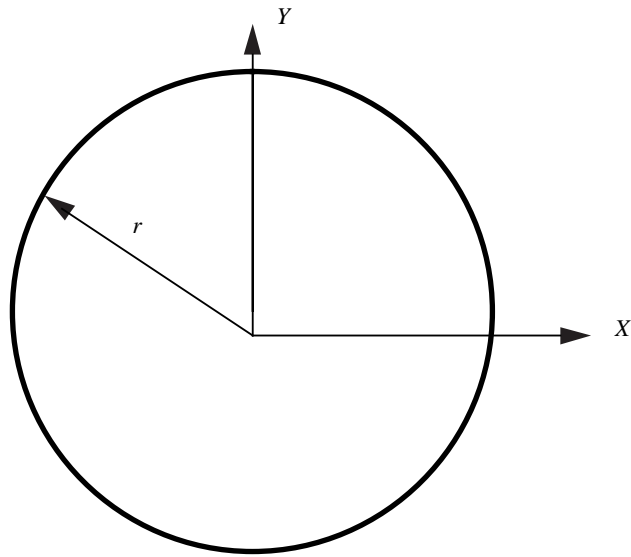
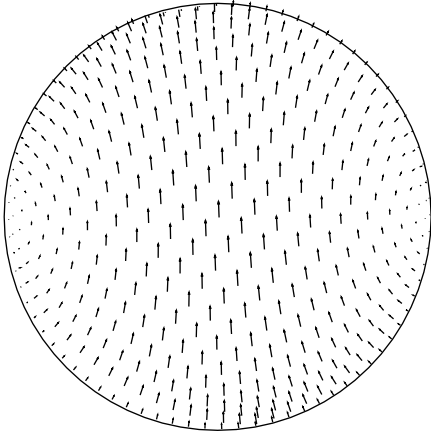
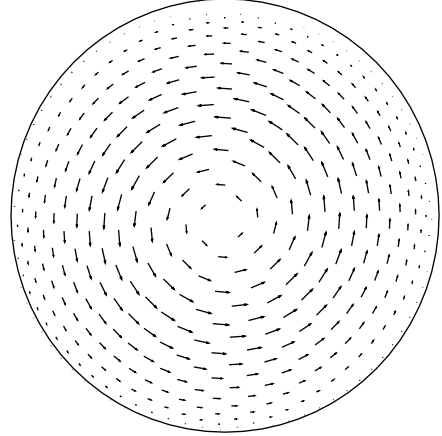


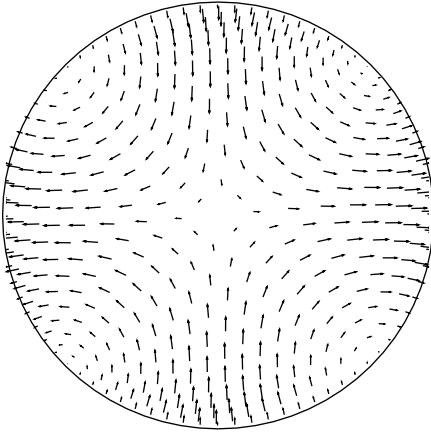
Figure 6. Cross section of circular waveguide.



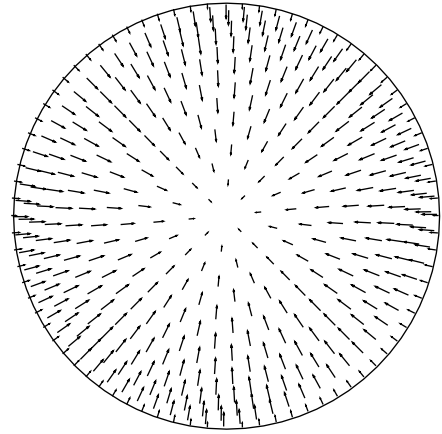
(a) TE_{11} mode.



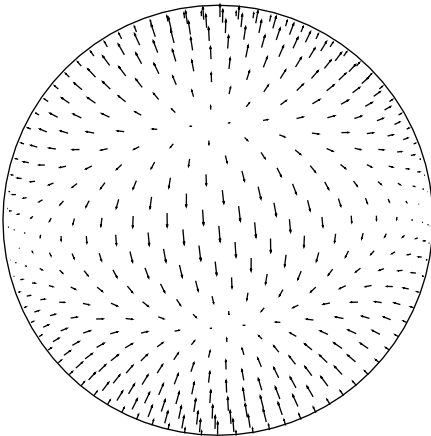
(b) TE_{01} mode.



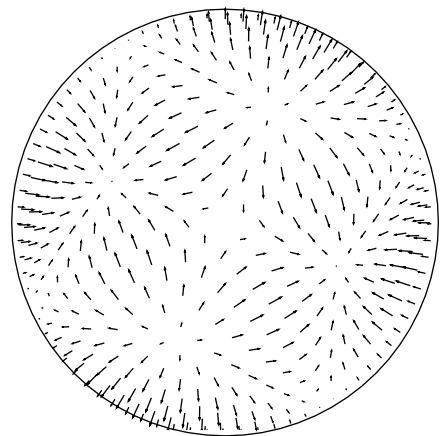
(c) TE_{21} mode.



(d) TM_{01} mode.



(e) TM_{11} mode.



(f) TM_{21} mode.

Figure 7. Electric field distribution of some modes for circular waveguide.

Table 3. Cutoff Wave Numbers for Coaxial Line With $r_2/r_1 = 4$

Mode	$k_c r_1$	
	Analytical (ref. 10)	HELM10
TE ₁₁	0.411	0.412
TE ₂₁	0.752	0.754
TE ₃₁	1.048	1.055
TM ₀₁	1.024	1.030
TM ₁₁	1.112	1.120

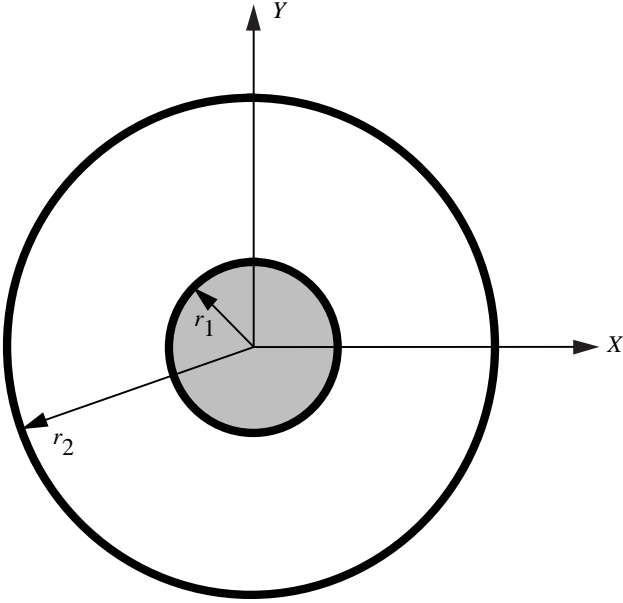


Figure 8. Cross section of coaxial line.

2.1.5. Summary

In section 2, a nodal-based two-dimensional finite element method has been described for homogeneous waveguides using Galerkin's technique. The procedure outlined here is valid for any arbitrary cross section of the waveguide filled with homogeneous materials. The HELM10 computer program gives the cutoff wave numbers and the transverse electric field components for any mode of propagation in such a waveguide. Examples of a rectangular waveguide, a circular waveguide, and a coaxial line are presented to validate the computer code. Accuracy of the numerical results depends on the number of elements used to represent the geometry.

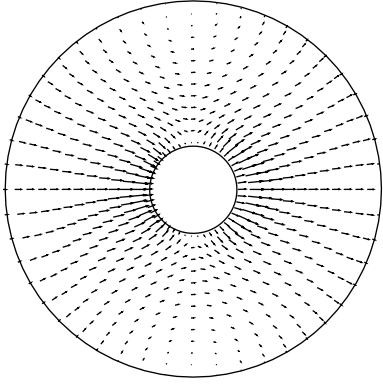
2.2. Inhomogeneous Waveguides—Vector Formulation

For inhomogeneous waveguide problems, the scalar potential approach is not applicable if one is

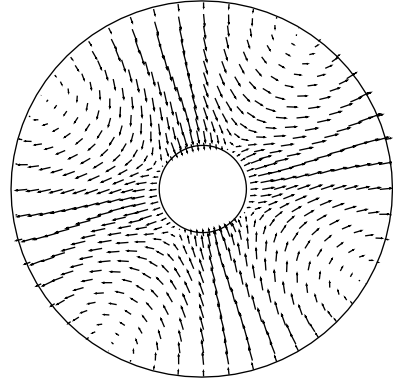
interested in the dispersion characteristics of the waveguide. For this a vector finite element approach has to be followed. Unfortunately, the nodal-based finite element method when applied to the vector wave equation results in nonphysical or spurious solutions, which are generally attributed to the lack of enforcement of divergence condition. (See refs. 2 and 11.) Many attempts have been made to avoid these spurious modes by different variations of the nodal-based finite element method. Fortunately, a revolutionary approach has been discovered recently. This approach uses the so-called “vector basis” or “vector elements,” which assign degrees of freedom to the edges rather than to the nodes of the element. For this reason they are popularly referred to as “edge elements.”

Although the edge elements were first described by Whitney (ref. 12) 35 years ago, their importance in electromagnetics was not realized until the late 1980's (ref. 3). In section 2.2, we describe the formulation of the finite element method for vector wave equation using edge elements. This formulation, in general, follows the one given by Lee, Sun, and Cendes (ref. 13). But instead of attempting to solve the dispersion problem right away, we use the following steps to build the edge element formulation:

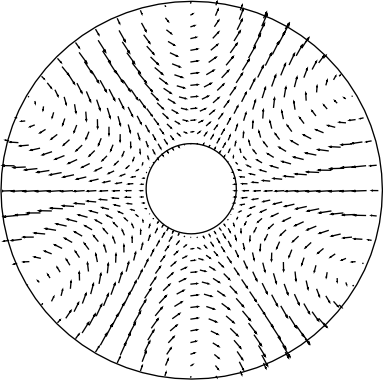
1. Solve for the homogeneous waveguide problem by using two-component transverse vector fields
2. Solve for the generalized waveguide problem by using three-component vector fields
3. Solve for the wave number k_o when the propagation constant β is specified
4. Solve for the propagation constant β of any generalized waveguide for a given frequency of operation



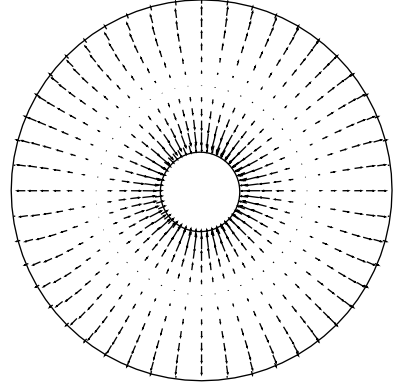
(a) TE_{11} mode.



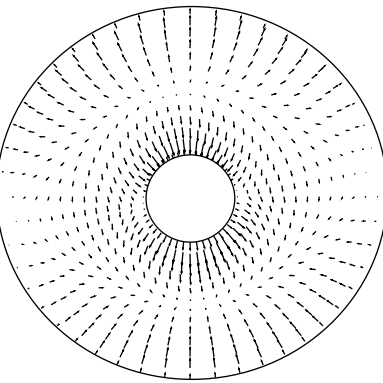
(b) TE_{21} mode.



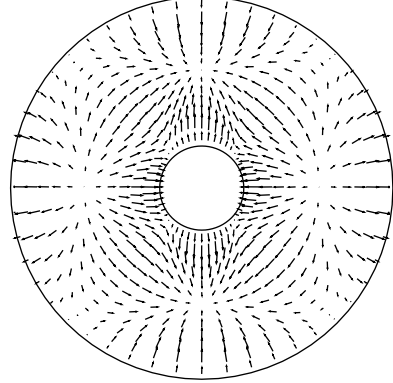
(c) TE_{31} mode.



(d) TM_{01} mode.



(e) TM_{11} mode.



(f) TM_{21} mode.

Figure 9. Electric field distribution of some modes for coaxial line.

2.2.1. Solution of Homogeneous Waveguide Problem With Two-Component Transverse Vector Fields

For a homogeneous waveguide, the propagating modes can be divided into transverse electric (TE) or transverse magnetic (TM) modes, which can be solved separately. For the TE mode $E_z = 0$, the transverse electric field vector \mathbf{E}_t satisfies the vector wave equation

$$\nabla_t \times \left(\frac{1}{\mu_r} \nabla_t \times \mathbf{E}_t \right) - k_c^2 \varepsilon_r \mathbf{E}_t = 0 \quad (42)$$

and for the TM mode $H_z = 0$, the transverse electric field vector \mathbf{H}_t satisfies the vector wave equation

$$\nabla_t \times \left(\frac{1}{\varepsilon_r} \nabla_t \times \mathbf{H}_t \right) - k_c^2 \mu_r \mathbf{H}_t = 0 \quad (43)$$

where μ_r and ε_r are the permeability and permittivity, respectively, of the material in the waveguide.

In this section, we illustrate the procedure for the TE mode and the same procedure can be applied for the TM mode, except the Neumann boundary conditions are applied at PEC boundaries instead of the Dirichlet boundary conditions.

2.2.1.1. Formulation. For the TE mode, reconsider the wave equation (42), which is

$$\nabla_t \times \left(\frac{1}{\mu_r} \nabla_t \times \mathbf{E}_t \right) - k_c^2 \varepsilon_r \mathbf{E}_t = 0$$

Dot multiplying equation (42) by a vector testing function \mathbf{T}_t and integrating over the cross section of the waveguide, we get

$$\iint_{\Gamma} \left(\mathbf{T}_t \cdot \nabla_t \times \left(\frac{1}{\mu_r} \nabla_t \times \mathbf{E}_t \right) - k_c^2 \varepsilon_r \mathbf{T}_t \cdot \mathbf{E}_t \right) ds = 0 \quad (44)$$

From the vector identities,

$$\mathbf{T}_t \cdot (\nabla_t \times \mathbf{A}) = (\nabla_t \times \mathbf{T}_t) \cdot \mathbf{A} - \nabla_t \cdot (\mathbf{T}_t \times \mathbf{A}) \quad (45)$$

$$(\mathbf{T}_t \times \mathbf{A}) \cdot \hat{n} = -\mathbf{T}_t \cdot (\hat{n} \times \mathbf{A}) \quad (46)$$

and the divergence theorem,

$$\iint_{\Gamma} \nabla_t \cdot (\mathbf{T}_t \times \mathbf{A}) ds = \int_{d\Gamma} (\mathbf{T}_t \times \mathbf{A}) \cdot \hat{n} dl \quad (47)$$

equation (44) can be written in weak form as

$$\begin{aligned} \iint_{\Gamma} \frac{1}{\mu_r} (\nabla_t \times \mathbf{T}_t) \cdot (\nabla_t \times \mathbf{E}_t) ds &= k_c^2 \varepsilon_r \iint_{\Gamma} \mathbf{T}_t \cdot \mathbf{E}_t ds \\ &- \int_{d\Gamma} \mathbf{T}_t \cdot \left(\hat{n} \times \frac{1}{\mu_r} \nabla_t \times \mathbf{E}_t \right) dl \end{aligned} \quad (48)$$

On a perfect electric conducting (PEC) boundary, the contour integral vanishes as \mathbf{T}_t is set to zero to satisfy the Dirichlet boundary conditions. Hence, for all the problems closed by PEC walls, the last term on the right-hand side of equation (48) is set to zero. Thus, the final equation can be written as

$$\iint_{\Gamma} \frac{1}{\mu_r} (\nabla_t \times \mathbf{T}_t) \cdot (\nabla_t \times \mathbf{E}_t) ds = k_c^2 \varepsilon_r \iint_{\Gamma} \mathbf{T}_t \cdot \mathbf{E}_t ds \quad (49)$$

2.2.1.2. Discretization. The finite elements used in section 2.1 are scalar and have unknown parameters, the values of the scalar field at the nodes of the element. Nodal-based finite elements are not suitable to represent vector fields in electromagnetics, as the boundary conditions often take the form of a specification of only the part of the vector field that is tangent to the boundary. With nodal-based elements, the physical constraint must be transformed into linear relationships between the Cartesian components, and at nodes where the boundary changes direction, an average tangential direction must be determined first. These are very difficult (if not impossible) to implement in nodal-based finite elements. The failure to implement proper conditions results in spurious modes which are nonphysical.

The most elegant and simple approach to eliminate the disadvantages of the nodal-based elements is to use edge elements. Edge elements are recently developed finite element bases for vector fields. With edge elements, only the tangential continuity of the vector fields is imposed across the element boundaries. The advantages of edge elements are as follows:

1. The edge elements impose the continuity of only the tangential components of the electric and magnetic fields, which is consistent with the physical constraints on these fields.
2. The interelement boundary conditions are automatically obtained through the natural boundary conditions.
3. The Dirichlet boundary condition can be easily imposed along the element edges.

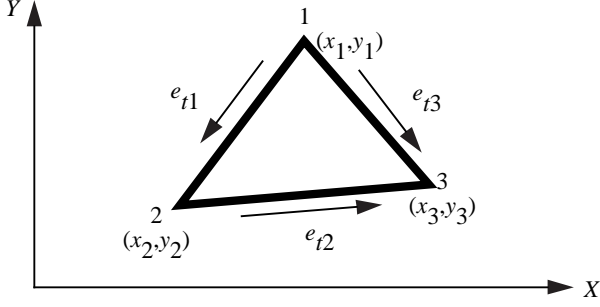


Figure 10. Configuration of tangential edge elements.

4. As the edge elements are chosen to be divergence free, the spurious nonphysical solutions are completely eliminated.

For a single triangular element shown in figure 10, the transverse electric field can be expressed as a superposition of edge elements. The edge elements permit a constant tangential component of the basis function along one triangular edge while simultaneously allowing a zero tangential component along the other two edges. Three such basis functions overlapping each triangular cell, provide the complete expansion (ref. 11):

$$\mathbf{E}_t = \sum_{m=1}^3 e_{tm} \mathbf{W}_{tm} \quad (50)$$

where

$$\mathbf{W}_{tm} = L_{tm}(\alpha_i \nabla_t \alpha_j - \alpha_j \nabla_t \alpha_i) \quad (51)$$

α_i is the first-order shape function associated with nodes 1, 2, and 3 defined by equation (15); and L_{tm} is the length of edge m connecting nodes i and j , that is, explicitly, the basis functions representing edges 1, 2, and 3 with coefficients e_{t1} , e_{t2} , and e_{t3} written as

$$\mathbf{W}_{t1} = L_{t1}(\alpha_1 \nabla_t \alpha_2 - \alpha_2 \nabla_t \alpha_1) \quad (52)$$

$$\mathbf{W}_{t2} = L_{t2}(\alpha_2 \nabla_t \alpha_3 - \alpha_3 \nabla_t \alpha_2) \quad (53)$$

$$\mathbf{W}_{t3} = L_{t3}(\alpha_3 \nabla_t \alpha_1 - \alpha_1 \nabla_t \alpha_3) \quad (54)$$

The three unknown parameters are e_{tm} . It can be shown that

$$\hat{t}_{tm} \cdot \mathbf{E}_t = e_{tm} \quad (\text{on edge } m) \quad (55)$$

where \hat{t}_{tm} is a unit vector along edge m in the direction of the edge; for example,

$$\hat{t}_{t1} = \frac{(x_2 - x_1)\hat{x} + (y_2 - y_1)\hat{y}}{L_{t1}}$$

for edge 1 connecting nodes 1 and 2. In other words, e_{tm} controls the tangential field on edge m . Later $\nabla_t \cdot \mathbf{W}_{tm} = 0$ is verified and hence the electric field obtained through equation (50) satisfies $\nabla_t \cdot \mathbf{E}_t = 0$, the divergence equation, within the element. Therefore, the finite element solution is free of spurious solutions.

With the use of the simplex coordinates as defined by equation (15), the basis function given by equation (51) can be written as

$$\mathbf{W}_{tm} = \frac{L_{tm}}{4\Delta^2} [(A_m + B_m y)\hat{x} + (C_m + D_m x)\hat{y}] \quad (56)$$

where

$$A_m = a_i b_j - a_j b_i \quad (57)$$

$$B_m = c_i b_j - c_j b_i \quad (58)$$

$$C_m = a_i c_j - a_j c_i \quad (59)$$

$$D_m = b_i c_j - b_j c_i = -B_m \quad (60)$$

From equation (56), $\nabla_t \cdot \mathbf{W}_{tm} = 0$, which results in a divergenceless electric field; that is, $\nabla_t \cdot \mathbf{E}_t = 0$.

2.2.1.3. Finite element formulation. Substituting equation (50) into equation (49) for a single triangular element gives the following equation:

$$\begin{aligned} & \frac{1}{\mu_r} \iint_{\Delta} \sum_{m=1}^3 (\nabla_t \times \mathbf{W}_{tm}) \cdot (\Delta_t \times \mathbf{W}_{tn}) e_{tm} ds \\ &= k_c^2 \varepsilon_r \iint_{\Delta} \sum_{m=1}^3 (\mathbf{W}_{tm} \cdot \mathbf{W}_{tn}) e_{tm} ds \\ & (n = 1, 2, 3) \end{aligned} \quad (61)$$

where Δ indicates the integration over the triangular element. By interchanging the integration and summations, equation (61) can be written in a matrix form as

$$[\mathbf{S}_{el}][e_t] = k_c^2 [\mathbf{T}_{el}][e_t] \quad (62)$$

Hence the finite element matrices for a single element are given by

$$[\mathbf{S}_{el}] = \frac{1}{\mu_r} \iint_{\Delta} (\nabla_t \times \mathbf{W}_{tm}) \cdot (\nabla_t \times \mathbf{W}_{tn}) ds \quad (63)$$

and

$$[\mathbf{T}_{el}] = \varepsilon_r \iint_{\Delta} (\mathbf{W}_{tm} \cdot \mathbf{W}_{tn}) ds \quad (64)$$

These element matrices can be assembled over all the triangles in the cross section of the waveguide to obtain a global eigenmatrix equation.

$$[\mathbf{S}][e_t] = k_c^2[\mathbf{T}][e_t] \quad (65)$$

2.2.1.4. Finite element matrices. Closed-form expressions for integrals in equations (63) and (64) can be written as

$$\iint_{\Delta} (\nabla_t \times \mathbf{W}_{tm}) \cdot (\nabla_t \times \mathbf{W}_{tn}) ds = \frac{L_{tm}L_{tn}}{4A^3} D_m D_n \quad (66)$$

and

$$\iint_{\Delta} (\mathbf{W}_{tm} \cdot \mathbf{W}_{tn}) ds = \frac{L_{tm}L_{tn}}{16A^3} (I_{t1} + I_{t2} + I_{t3} + I_{t4} + I_{t5}) \quad (67)$$

where

$$I_{t1} = \frac{1}{A} (A_m A_n + C_m C_n) \iint_{\Delta} dx dy \quad (68)$$

$$I_{t2} = \frac{1}{A} (C_m D_n + C_n D_m) \iint_{\Delta} x dx dy \quad (69)$$

$$I_{t3} = \frac{1}{A} (A_m B_n + A_n B_m) \iint_{\Delta} y dx dy \quad (70)$$

$$I_{t4} = \frac{1}{A} (B_m B_n) \iint_{\Delta} y^2 dx dy \quad (71)$$

$$I_{t5} = \frac{1}{A} (D_m D_n) \iint_{\Delta} x^2 dx dy \quad (72)$$

These equations can be reduced further by the following integration formulas for integrating over a triangle given in reference 14:

$$I_{t1} = (A_m A_n + C_m C_n) \quad (73)$$

$$I_{t2} = (C_m D_n + C_n D_m) \bar{x}_{\text{tri}} \quad (74)$$

$$I_{t3} = (A_m B_n + A_n B_m) \bar{y}_{\text{tri}} \quad (75)$$

$$I_{t4} = \frac{B_m B_n}{12} \left(\sum_{i=1}^3 y_i^2 + 9 \bar{y}_{\text{tri}}^2 \right) \quad (76)$$

$$I_{t5} = \frac{D_m D_n}{12} \left(\sum_{i=1}^3 x_i^2 + 9 \bar{x}_{\text{tri}}^2 \right) \quad (77)$$

2.2.1.5. Numerical examples. A computer program HELMVEC was written to solve the eigenvalue problem presented in section 2.2.1. Numerical data computed with this program for a rectangular waveguide and a circular waveguide are given as follows.

Rectangular waveguide: The cutoff wave numbers of an air-filled rectangular waveguide (shown in fig. 4, $a_r/b_r = 2$) were calculated with the procedure in section 2.2.1 (HELMVEC) and are presented in table 4 for both the TE and TM modes along with analytical data from reference 9. Four hundred triangular elements have been used to represent the geometry.

Table 4. Cutoff Wave Numbers for Rectangular Waveguide

Mode	$k_c a_r$	
	Analytical (ref. 9)	HELMVEC
TE mode		
TE ₁₀	3.142	3.140
TE ₂₀	6.285	6.274
TE ₃₀	9.428	9.396
TE ₀₁	6.285	6.274
TE ₁₁	7.027	7.024
TE ₂₁	8.889	8.897
TE ₃₁	11.331	11.339
TE ₀₂	12.571	12.497
TM mode		
TM ₁₁	7.027	7.024
TM ₁₂	8.889	8.889
TM ₁₃	11.331	11.340
TM ₂₁	12.958	12.902
TM ₂₂	14.055	14.044
TM ₂₃	15.710	15.757
TM ₃₁	19.117	18.906
TM ₃₂	19.877	19.728

Circular waveguide: The cutoff wave numbers for an air-filled circular waveguide (Radius = 1) were also computed by HELMVEC and compared with analytically calculated values from reference 9. These results are presented in table 5 for both the TE and TM modes. The waveguide geometry is represented by 200 triangular elements.

2.2.2. Inhomogeneous Waveguide Problems Using Three-Component Vector Fields

In this section, a generalized approach for finding the cutoff frequencies of inhomogeneously filled waveguides is described.

Table 5. Cutoff Wave Numbers for Circular Waveguide

Mode	k_c	
	Analytical (ref. 9)	HELMVEC
TE mode		
TE ₀₁	3.832	3.834
TE ₁₁	1.841	1.846
TE ₁₂	3.054	3.070
TE ₁₃	4.201	4.192
TE ₂₀	7.016	7.002
TE ₂₁	5.331	5.332
TE ₂₂	6.706	6.620
TE ₂₃	8.015	8.178
TM mode		
TM ₁₀	2.405	2.416
TM ₁₁	3.832	3.831
TM ₁₂	5.136	5.155
TM ₁₃	6.380	6.358
TM ₂₀	5.520	5.508
TM ₂₁	7.016	7.054
TM ₂₂	8.417	8.403
TM ₂₃	9.761	9.644

2.2.2.1. Formulation. This generalized approach can be followed by using either the \mathbf{E} or \mathbf{H} field. We will illustrate the case for the \mathbf{E} field. The vector wave equation for \mathbf{E} is given by

$$\nabla_t \times \left(\frac{1}{\mu_r} \nabla_t \times \mathbf{E} \right) - k_c^2 \varepsilon_r \mathbf{E} = 0 \quad (78)$$

The electric field can be written as

$$\mathbf{E} = \mathbf{E}_t + \hat{z} E_z \quad (79)$$

Hence equation (78) can be divided into two parts—one consisting of the transverse electric fields and the other, the z -component of the electric field—that is,

$$\nabla_t \times \left(\frac{1}{\mu_r} \nabla_t \times \mathbf{E}_t \right) - k_c^2 \varepsilon_r \mathbf{E}_t = 0 \quad (80)$$

$$\nabla_t \cdot \frac{1}{\mu_r} \nabla_t E_z + k_c^2 \varepsilon_r E_z = 0 \quad (81)$$

Equation (80) can be written in its weak form as

$$\iint_{\Gamma} \frac{1}{\mu_r} (\nabla_t \times \mathbf{T}_t) \cdot (\nabla_t \times \mathbf{E}_t) ds = k_c^2 \varepsilon_r \iint_{\Gamma} \mathbf{T}_t \cdot \mathbf{E}_t ds \quad (82)$$

and equation (81) can be written in its weak form by following equations (2) through (7) to obtain

$$\iint_{\Gamma} \frac{1}{\mu_r} (\nabla_t T_z \cdot \nabla_t E_z) ds = k_c^2 \varepsilon_r \iint_{\Gamma} T_z E_z ds \quad (83)$$

where the testing function is $\mathbf{T} = \mathbf{T}_t + \hat{z} T_z$.

2.2.2.2. Discretization. As the vector Helmholtz equation is divided into two parts, vector-based tangential edge elements can be used to approximate the transverse fields, and nodal-based first-order Lagrangian interpolation functions can be used to approximate the z -component. From equation (50), which is

$$\mathbf{E}_t = \sum_{m=1}^3 e_{tm} \mathbf{W}_{tm}$$

where m indicates the m th edge of the triangle and \mathbf{W}_{tm} is the edge element for edge m . The testing function \mathbf{T}_t is chosen to be the same as the basis function in equation (50) (shown above); that is, $\mathbf{T}_t = \mathbf{W}_{tm}$. The z -component of the electric field can be written as

$$E_z = \sum_{i=1}^3 e_{zi} \alpha_i \quad (84)$$

Here i indicates i th node and α_i is the simplex coordinate of node i as given in equation (15). Also the testing function \mathbf{T}_z is chosen to be the same as the basis function in equation (84); that is, $\mathbf{T}_z = \alpha_j$.

2.2.2.3. Finite element formulation. Substituting equations (50) and (84) into equations (82) and (83), respectively, we can get the following equations:

$$\begin{aligned} & \frac{1}{\mu_r} \iint_{\Delta} \sum_{m=1}^3 (\nabla_t \times \mathbf{W}_{tm}) \cdot (\nabla_t \times \mathbf{W}_{tn}) e_{tm} ds \\ &= k_c^2 \varepsilon_r \iint_{\Delta} \sum_{m=1}^2 (\mathbf{W}_{tm} \cdot \mathbf{W}_{tn}) e_{tm} ds \\ & (n = 1, 2, 3) \end{aligned} \quad (85)$$

$$\begin{aligned} & \frac{1}{\mu_r} \sum_{i=1}^3 e_{zi} \iint_{\Delta} (\nabla_t \alpha_i \cdot \nabla_t \alpha_j) dx dy \\ &= k_c^2 \varepsilon_r \sum_{i=1}^3 e_{zi} \iint_{\Delta} \alpha_i \alpha_j dx dy \quad (j = 1, 2, 3) \end{aligned} \quad (86)$$

By interchanging the summation and integration in equation (85), these two equations can be combined to be written in a matrix form as

$$\begin{bmatrix} S_{\text{el}(t)} & 0 \\ 0 & S_{\text{el}(z)} \end{bmatrix} \begin{bmatrix} e_t \\ e_z \end{bmatrix} = k_c^2 \begin{bmatrix} T_{\text{el}(t)} & 0 \\ 0 & T_{\text{el}(z)} \end{bmatrix} \begin{bmatrix} e_t \\ e_z \end{bmatrix} \quad (87)$$

Hence the element matrices are given by

$$S_{\text{el}(t)} = \frac{1}{\mu_r} \iint_{\Delta} (\nabla_t \times \mathbf{W}_{tm}) \cdot (\nabla_t \times \mathbf{W}_{tn}) ds \quad (88)$$

$$S_{\text{el}(z)} = \frac{1}{\mu_r} \iint_{\Delta} (\nabla \alpha_i \cdot \nabla \alpha_j) dx dy \quad (89)$$

$$T_{\text{el}(t)} = \varepsilon_r \iint_{\Delta} (\mathbf{W}_{tm} \cdot \mathbf{W}_{tn}) ds \quad (90)$$

$$T_{\text{el}(z)} = \varepsilon_r \iint_{\Delta} \alpha_i \alpha_j dx dy \quad (91)$$

These element matrices can be assembled over all the triangles in the cross section of the waveguide to obtain a global eigenmatrix equation:

$$\begin{bmatrix} S_t & 0 \\ 0 & S_z \end{bmatrix} \begin{bmatrix} e_t \\ e_z \end{bmatrix} = k^2 \begin{bmatrix} T_t & 0 \\ 0 & T_z \end{bmatrix} \begin{bmatrix} e_t \\ e_z \end{bmatrix} \quad (92)$$

2.2.2.4. Finite element matrices. The finite element matrices shown in equations (88) through (91) are already derived in the previous sections. Equation (88) is given by equation (66), equation (89) by equation (31), equation (90) by equation (67), and equation (91) by equation (33).

2.2.2.5. Numerical examples. A computer program HELMVEC1 was written for the three-component vector formulation to calculate cutoff wave numbers of waveguides with arbitrary cross sections. Numerical data computed with HELMVEC1 for a rectangular waveguide and a circular waveguide are given as follows.

Rectangular waveguide: The cutoff wave numbers of an air-filled rectangular waveguide (shown in fig. 4, $a_r/b_r = 2$) are calculated with the procedure in section 2.2.2 (HELMVEC1) and are presented in table 6 along with analytical data from reference 9. In the present formulation, it is not required to calculate eigenvalues separately for TE and TM modes. Both **E** and **H** formulations result in almost identical numerical results.

Circular waveguide: The cutoff wave numbers for an air-filled circular waveguide (Radius = 1) are also computed and compared with analytically calculated values. These are given in table 7.

Table 6. Cutoff Wave Numbers for Rectangular Waveguide

Mode	$k_{c a_r}$		
	Analytical (ref. 9)	HELMVEC1 for—	
		E	H
TE mode			
TE ₁₀	3.142	3.142	3.144
TE ₂₀	6.285	6.274	6.308
TE ₃₀	9.428	9.396	9.511
TE ₀₁	6.285	6.274	6.308
TE ₁₁	7.027	7.024	7.024
TE ₂₁	8.889	8.897	8.897
TE ₃₁	11.331	11.339	11.340
TE ₀₂	12.571	12.497	12.772
TM mode			
TM ₁₁	7.027	7.072	7.207
TM ₂₁	8.889	8.995	8.993
TM ₃₁	11.331	11.541	11.537
TM ₀₂	12.571	12.498	12.772

Table 7. Cutoff Wave Numbers for Circular Waveguide

Mode	k_c		
	Analytical (ref. 9)	HELMVEC1 for—	
		E	H
TE mode			
TE ₀₁	3.832	3.798	3.891
TE ₁₁	1.841	1.869	1.875
TE ₁₂	3.054	3.092	3.172
TE ₁₃	4.201	4.258	4.084
TE ₂₀	7.016	6.899	6.912
TE ₂₁	5.331	5.426	5.226
TE ₂₂	6.706	6.653	6.746
TE ₂₃	8.015	7.930	8.116
TM mode			
TM ₁₀	2.405	2.481	2.439
TM ₁₁	3.832	3.798	3.891
TM ₁₂	5.136	5.228	5.183
TM ₁₃	6.380	6.507	6.335
TM ₂₀	5.520	5.493	5.551
TM ₂₁	7.016	7.490	7.410
TM ₂₂	8.417	8.591	8.449
TM ₂₃	9.761	9.769	9.804

2.2.3. Wave-Number Determination for Given Propagation Constant

A generalized approach for finding the wave number k_o is described for a given propagation constant β .

2.2.3.1. Formulation. Again the same approach as used earlier can be followed by using either the \mathbf{E} or \mathbf{H} field. We illustrate the case for the \mathbf{E} field, which is the same for the \mathbf{H} field. The vector wave equation for the \mathbf{E} field is given by

$$\nabla \times \left(\frac{1}{\mu_r} \nabla \times \mathbf{E} \right) - k_o^2 \varepsilon_r \mathbf{E} = 0 \quad (93)$$

where $\mathbf{E} = (E_x \hat{x} + E_y \hat{y} + E_z \hat{z}) \exp(-j\beta z)$. By doing the curl-curl operation and separating the transverse from the longitudinal components, equation (93) can be divided into two equations and rewritten as

$$\nabla_t \times \left(\frac{1}{\mu_r} \nabla_t \times \mathbf{E}_t \right) - \frac{1}{\mu_r} (j\beta \nabla_t E_z - \beta^2 \mathbf{E}_t) = k_o^2 \varepsilon_r \mathbf{E}_t \quad (94)$$

$$-\frac{1}{\mu_r} [\nabla_t \cdot (\nabla_t E_z + j\beta \mathbf{E}_t)] = k_o^2 \varepsilon_r E_z \quad (95)$$

and $\mathbf{E}_t = E_x \hat{x} + E_y \hat{y}$. Separate β from k_o^2 and to have real-valued matrices introduce the scaling

$$\mathbf{E}_t = \frac{\mathbf{E}_t}{\beta} \quad (96)$$

$$E_z = \frac{-E_z}{j} \quad (97)$$

Then equations (94) and (95) can be written as

$$\nabla_t \times \left(\frac{1}{\mu_r} \nabla_t \times \mathbf{E}_t \right) + \frac{1}{\mu_r} (\beta^2 \nabla_t E_z + \beta^2 \mathbf{E}_t) = k_o^2 \varepsilon_r \mathbf{E}_t \quad (98)$$

$$-\frac{1}{\mu_r} [\nabla_t \cdot (\nabla_t E_z + \mathbf{E}_t)] = k_o^2 \varepsilon_r E_z \quad (99)$$

To apply Galerkin's method to equations (98) and (99), multiply equation (98) with the testing function \mathbf{T}_t and equation (99) with the testing function T_z and integrate both the equations over the cross section of the waveguide Γ ; that is,

$$\begin{aligned} & \int_{\Gamma} \left[\mathbf{T}_t \cdot \nabla_t \times \left(\frac{1}{\mu_r} \nabla_t \times \mathbf{E}_t \right) + \frac{\beta^2}{\mu_r} (\mathbf{T}_t \cdot \nabla_t E_z + \mathbf{T}_t \cdot \mathbf{E}_t) \right] ds \\ &= k_o^2 \varepsilon_r \int_{\Gamma} \mathbf{T}_t \cdot \mathbf{E}_t ds \end{aligned} \quad (100)$$

$$-\frac{1}{\mu_r} \int_{\Gamma} T_z [\nabla_t \cdot (\nabla_t E_z + \mathbf{E}_t)] ds = k_o^2 \varepsilon_r \int_{\Gamma} T_z E_z ds \quad (101)$$

With the vector identities

$$\mathbf{A} \cdot (\nabla_t \times \mathbf{B}) = (\nabla_t \times \mathbf{A}) \cdot \mathbf{B} - \nabla_t \cdot (\mathbf{A} \times \mathbf{B}) \quad (102)$$

$$\int_{\Gamma} \nabla_t \cdot (\mathbf{A} \times \mathbf{B}) ds = \int_{d\Gamma} (\mathbf{A} \times \mathbf{B}) \cdot \hat{n} dl = - \int_{d\Gamma} \mathbf{A} \cdot (\hat{n} \times \mathbf{B}) dl \quad (103)$$

$$\nabla_t \cdot f \mathbf{A} = \mathbf{A} \cdot \nabla_t f + f \nabla_t \cdot \mathbf{A} \quad (104)$$

$$\int_{\Gamma} \nabla_t \cdot \mathbf{A} ds = \int_{d\Gamma} \mathbf{A} \cdot \hat{n} dl \quad (105)$$

equations (100) and (101) can be written in their weak form as

$$\begin{aligned} & \frac{1}{\mu_r} \int_{\Gamma} [(\nabla_t \times \mathbf{T}_t) \cdot (\nabla_t \times \mathbf{E}_t) + (\beta^2 \mathbf{T}_t \cdot \nabla E_z + \beta^2 \mathbf{T}_t \cdot \mathbf{E}_t)] ds \\ &= k_o^2 \varepsilon_r \int_{\Gamma} \mathbf{T}_t \cdot \mathbf{E}_t ds - \frac{1}{\mu_r} \int_{d\Gamma} \mathbf{T}_t \cdot (\hat{n} \times \nabla \times \mathbf{E}_t) ds \end{aligned} \quad (106)$$

$$\begin{aligned} & \frac{1}{\mu_r} \int_{\Gamma} (\nabla_t T_z \cdot \nabla_t E_z + \nabla_t T_z \cdot \mathbf{E}_t) ds \\ &= k_o^2 \varepsilon_r \int_{\Gamma} T_z E_z ds + \frac{1}{\mu_r} \int_{d\Gamma} T_z \frac{\partial E_z}{\partial n} + T_z \hat{n} \cdot \mathbf{E}_t ds \end{aligned} \quad (107)$$

If the waveguide boundary $d\Gamma$ is assumed to be perfectly conducting, then $\mathbf{T}_t = 0$ and $T_z = 0$ on $d\Gamma$. Hence, the line integrals on the right-hand side of equations (106) and (107) can be neglected. Multiplying equation (107) with β^2 for the sake of symmetry, equations (106) and (107) can be rewritten as

$$\begin{aligned} & \frac{1}{\mu_r} \int_{\Gamma} [(\nabla_t \times \mathbf{T}_t) \cdot (\nabla_t \times \mathbf{E}_t) \\ &+ (\beta^2 \mathbf{T}_t \cdot \nabla E_z + \beta^2 \mathbf{T}_t \cdot \mathbf{E}_t)] ds \\ &= k_o^2 \varepsilon_r \int_{\Gamma} \mathbf{T}_t \cdot \mathbf{E}_t ds \end{aligned} \quad (108)$$

$$\begin{aligned} & \frac{\beta^2}{\mu_r} \iint_{\Gamma} (\nabla_t T_z \cdot \nabla_t E_z + \nabla_t T_z \cdot \mathbf{E}_t) ds \\ & = k_o^2 \beta^2 \varepsilon_r \iint_{\Gamma} T_z E_z ds \end{aligned} \quad (109)$$

2.2.3.2. Discretization. As the vector Helmholtz equation is divided into two parts, vector-based tangential edge elements can be used to approximate the transverse fields, and nodal-based first-order Lagrangian interpolation functions can be used to approximate the z -component. From equation (50), which is

$$\mathbf{E}_t = \sum_{m=1}^3 e_{tm} \mathbf{W}_{tm}$$

where m indicates the m th edge of the triangle and \mathbf{W}_{tm} is the edge element for edge m . The testing function \mathbf{T}_t is chosen to be the same as the basis function in equation (50); that is, $\mathbf{T}_t = \mathbf{W}_{tm}$. The z -component can be written as

$$E_z = \sum_{i=1}^3 e_{zi} \alpha_i$$

(This equation is eq. (84).) Here i indicates i th node and α_i is the simplex coordinate of node i as given in equation (15). Also the testing function \mathbf{T}_z is chosen to be the same as the basis function in equation (85) (given above); that is, $\mathbf{T}_z = \alpha_i$.

2.2.3.3. Finite element formulation. Substituting equations (50) and (84) into equations (108) and (109), respectively, integrating over a single triangular element, and interchanging the integration and summation give

$$\begin{aligned} & \frac{1}{\mu_r} \sum_{m=1}^3 \iint_{\Delta} (\nabla_t \times \mathbf{W}_{tm}) \cdot (\nabla_t \times \mathbf{W}_{tn}) e_{tm} ds \\ & + \frac{\beta^2}{\mu_r} \sum_{m=1}^3 \iint_{\Delta} (\mathbf{W}_{tm} \cdot \nabla \alpha_j) e_{zj} ds \\ & + \frac{\beta^2}{\mu_r} \sum_{m=1}^3 \iint_{\Delta} (\mathbf{W}_{tm} \cdot \mathbf{W}_{tn}) e_{tm} ds \\ & = k_o^2 \sum_{m=1}^3 \varepsilon_r \iint_{\Delta} (\mathbf{W}_{tm} \cdot \mathbf{W}_{tn}) e_{tm} ds \\ & (n = 1, 2, 3; j = 1, 2, 3) \end{aligned} \quad (110)$$

$$\begin{aligned} & \frac{\beta^2}{\mu_r} \sum_{i=1}^3 \iint_{\Delta} (\nabla \alpha_i \cdot \nabla \alpha_j) e_{zi} ds \\ & + \frac{\beta^2}{\mu_r} \sum_{i=1}^3 \iint_{\Delta} (\nabla \alpha_i \cdot \mathbf{W}_{tn}) e_{tn} ds \\ & = k_o^2 \sum_{i=1}^3 \beta^2 \varepsilon_r \iint_{\Gamma} \alpha_i \alpha_j e_{zi} ds \\ & (j = 1, 2, 3; n = 1, 2, 3) \end{aligned} \quad (111)$$

Subscripts for α indicate node numbers and subscripts for \mathbf{W}_t indicate edge numbers. Equations (110) and (111) can be written in matrix form as

$$\begin{bmatrix} S_{\text{el}(tt)} & S_{\text{el}(tz)} \\ S_{\text{el}(zt)} & S_{\text{el}(zz)} \end{bmatrix} \begin{bmatrix} e_t \\ e_z \end{bmatrix} = k_o^2 \begin{bmatrix} T_{\text{el}(tt)} & 0 \\ 0 & T_{\text{el}(zz)} \end{bmatrix} \begin{bmatrix} e_t \\ e_z \end{bmatrix} \quad (112)$$

The element matrices are given by

$$\begin{aligned} S_{\text{el}(tt)} & = \frac{1}{\mu_r} \iint_{\Delta} (\nabla_t \times \mathbf{W}_{tm}) \cdot (\nabla_t \times \mathbf{W}_{tn}) ds \\ & + \frac{\beta^2}{\mu_r} \iint_{\Delta} (\mathbf{W}_{tm} \cdot \mathbf{W}_{tn}) ds \end{aligned} \quad (113)$$

$$S_{\text{el}(tz)} = \frac{\beta^2}{\mu_r} \iint_{\Delta} (\mathbf{W}_{tm} \cdot \nabla \alpha_j) ds \quad (114)$$

$$S_{\text{el}(zt)} = \frac{\beta^2}{\mu_r} \iint_{\Delta} (\nabla \alpha_i \cdot \mathbf{W}_{tn}) ds \quad (115)$$

$$S_{\text{el}(zz)} = \frac{\beta^2}{\mu_r} \iint_{\Delta} (\nabla \alpha_i \cdot \nabla \alpha_j) ds \quad (116)$$

$$T_{\text{el}(tt)} = \varepsilon_r \iint_{\Delta} (\mathbf{W}_{tm} \cdot \mathbf{W}_{tn}) ds \quad (117)$$

$$T_{\text{el}(zz)} = \beta^2 \varepsilon_r \iint_{\Delta} \alpha_i \alpha_j ds \quad (118)$$

These element matrices can be assembled over all the triangles in the cross section of the waveguide to obtain a global eigenvalue equation as follows:

$$\begin{bmatrix} S_{tt} & S_{tz} \\ S_{zt} & S_{zz} \end{bmatrix} \begin{bmatrix} e_t \\ e_z \end{bmatrix} = k_o^2 \begin{bmatrix} T_{tt} & 0 \\ 0 & T_{zz} \end{bmatrix} \begin{bmatrix} e_t \\ e_z \end{bmatrix} \quad (119)$$

2.2.3.4. *Finite element matrices.* Closed-form expressions are derived for the finite element matrices in equations (113) through (117). From equations (66) and (67),

$$S_{\text{el}(tt)} = \frac{1}{\mu_r} \left[\frac{L_{tm}L_{tn}}{16A^3} \left(D_m D_n + \sum_{k=1}^5 I_{tk} \right) \right] \quad (120)$$

With equations (73) through (77) and the procedures in sections 2.2.1 and 2.2.2, the remaining element matrices are derived as follows:

$$S_{\text{el}(tz)} = \frac{\beta^2}{\mu_r} \frac{L_{tm}}{8A^2} [b_j(A_m + B_m \bar{y}_{\text{tri}}) + c_j(C_m + D_m \bar{x}_{\text{tri}})] \quad (121)$$

$$S_{\text{el}(zt)} = \frac{\beta^2}{\mu_r} \frac{L_{tn}}{8A^2} [b_i(A_n + B_n \bar{y}_{\text{tri}}) + c_i(C_n + D_n \bar{x}_{\text{tri}})] \quad (122)$$

$$S_{\text{el}(zz)} = \frac{\beta^2}{\mu_r} \frac{b_i b_j + c_i c_j}{4A} \quad (123)$$

$$T_{\text{el}(tt)} = \varepsilon_r \frac{L_{tm}L_{tn}}{16A^3} \sum_{k=1}^5 I_{tk} \quad (124)$$

$$\left. \begin{aligned} T_{\text{el}(zz)} &= \beta^2 \varepsilon_r \frac{A}{6} & (m = n) \\ &= \beta^2 \varepsilon_r \frac{A}{12} & (m \neq n) \end{aligned} \right\} \quad (125)$$

2.2.3.5. *Numerical example.* A computer program HELMVEC2 was written to calculate the wave number of any generalized waveguide structure for a given propagation constant. To check the validity of the procedure, the first 10 wave numbers with $\beta = 10$ for LSM modes of a partially filled square waveguide (fig. 11) have been obtained by HELMVEC2 and compared with the available results in the literature (ref. 15). (See table 8.) The geometry is modelled by 72 triangular elements.

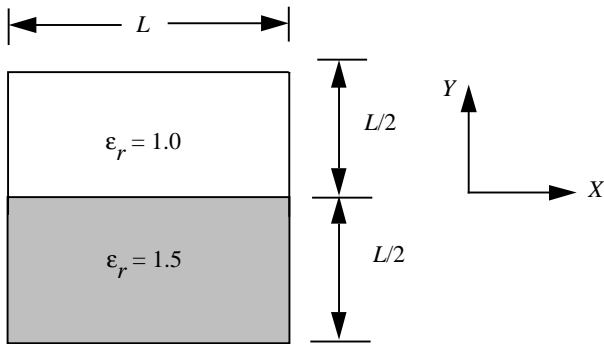


Figure 11. Partially filled square waveguide.

Table 8. Wave Numbers for LSM Modes of Square Waveguide With $\beta = 10$

Mode	$k_o L$	
	HELMVEC2	Hayata et al. (ref. 15)
1	8.815	8.8093
2	9.443	9.3896
3	10.35	10.2752
4	11.141	11.103
5	11.2890	11.2677
6	11.4246	11.4501
7	12.146	11.9882
8	12.5894	12.6686
9	12.8237	12.8092
10	12.9987	12.9575

2.2.4. Dispersion Characteristics of Waveguides

This section is simply an extension of section 2.2.3. The finite element equations are rearranged to obtain β when the operating frequency (or the wave number) is specified.

2.2.4.1. *Formulation.* The weak form derived in section 2.2.3.1 can be rearranged and equations (108) and (109) can be written as

$$\begin{aligned} & \frac{1}{\mu_r} \iint_{\Gamma} (\nabla_t \times \mathbf{T}_t) \cdot (\nabla_t \times \mathbf{E}_t) ds - k_o^2 \varepsilon_r \iint_{\Gamma} \mathbf{T}_t \cdot \mathbf{E}_t ds \\ &= -\frac{\beta^2}{\mu_r} \left(\iint_{\Gamma} \mathbf{T}_t \cdot \nabla_t E_z ds + \iint_{\Gamma} \mathbf{T}_t \cdot \mathbf{E}_t ds \right) \end{aligned} \quad (126)$$

$$\begin{aligned} & \frac{\beta^2}{\mu_r} \iint_{\Gamma} \nabla_t T_z \cdot \nabla_t E_z ds + \frac{\beta^2}{\mu_r} \iint_{\Gamma} \nabla_t T_z \cdot \mathbf{E}_t ds \\ &= k_o^2 \beta^2 \varepsilon_r \iint_{\Gamma} T_z E_z ds \end{aligned} \quad (127)$$

2.2.4.2. *Discretization.* As the vector Helmholtz equation is divided into two parts, vector-based tangential edge elements can be used to approximate the transverse fields, and nodal-based first-order Lagrangian interpolation functions can be used to approximate the z -component. From equation (50), which is

$$\mathbf{E}_t = \sum_{m=1}^3 e_{tm} \mathbf{W}_{tm}$$

where m indicates the m th edge of the triangle and \mathbf{W}_{tm} is the edge element for edge m . The testing function \mathbf{T}_t is chosen to be the same as the basis function in equation (127); that is, $\mathbf{T}_t = \mathbf{W}_{tm}$. The z -component is written as

$$E_z = \sum_{i=1}^3 e_{zi} \alpha_i$$

(which is eq. (84)). Here i indicates i th node and α_i is the simplex coordinate of node i as given in equation (15). Also the testing function \mathbf{T}_z is chosen to be the same as the basis function in equation (50) (given above); that is, $\mathbf{T}_z = \alpha_i$.

2.2.4.3. Finite element formulation. Substituting equations (127) and (50) into equations (125) and (126), respectively, integrating over a single triangular element, and interchanging the integration and summation give

$$\begin{aligned} & \frac{1}{\mu_r} \sum_{m=1}^3 \int_{\Delta} (\nabla_t \times \mathbf{W}_{tm}) \cdot (\nabla_t \times \mathbf{W}_{tn}) e_{tm} \\ & \times ds - k_o^2 \sum_{m=1}^3 \varepsilon_r \int_{\Delta} (\mathbf{W}_{tm} \cdot \mathbf{W}_{tn}) e_{tm} ds \\ & = -\beta^2 \left[\frac{1}{\mu_r} \sum_{m=1}^3 \int_{\Delta} (\mathbf{W}_{tm} \cdot \nabla \alpha_j) e_{zj} ds \right. \\ & \left. + \frac{1}{\mu_r} \sum_{m=1}^3 \int_{\Delta} (\mathbf{W}_{tm} \cdot \mathbf{W}_{tn}) e_{tm} ds \right] \\ & (n = 1, 2, 3; j = 1, 2, 3) \end{aligned} \quad (128)$$

$$\begin{aligned} & \frac{\beta^2}{\mu_r} \sum_{i=1}^3 \int_{\Delta} (\nabla \alpha_i \cdot \nabla \alpha_j) e_{zi} ds \\ & + \frac{\beta^2}{\mu_r} \sum_{i=1}^3 \int_{\Delta} (\nabla \alpha_i \cdot \mathbf{W}_{tn}) e_{tn} ds \\ & = \beta^2 \sum_{i=1}^3 k_o^2 \varepsilon_r \int_{\Delta} \alpha_i \alpha_j e_{zi} ds \\ & (j = 1, 2, 3; n = 1, 2, 3) \end{aligned} \quad (129)$$

Subscripts for α indicate node numbers and subscripts for \mathbf{W}_t indicate edge numbers. Equations (84)

and (128) can be written in matrix form as

$$\begin{bmatrix} S_{\text{el}(tt)} & 0 \\ 0 & 0 \end{bmatrix} \begin{bmatrix} e_t \\ e_z \end{bmatrix} = -\beta^2 \begin{bmatrix} T_{\text{el}(tt)} & T_{\text{el}(tz)} \\ T_{\text{el}(zt)} & T_{\text{el}(zz)} \end{bmatrix} \begin{bmatrix} e_t \\ e_z \end{bmatrix} \quad (130)$$

The element matrices are given by

$$\begin{aligned} S_{\text{el}(tt)} &= \frac{1}{\mu_r} \int_{\Delta} (\nabla_t \times \mathbf{W}_{tm}) \cdot (\nabla_t \times \mathbf{W}_{tn}) ds \\ & - k_o^2 \varepsilon_r \int_{\Delta} (\mathbf{W}_{tm} \cdot \mathbf{W}_{tn}) ds \end{aligned} \quad (131)$$

$$T_{\text{el}(tt)} = \varepsilon_r \int_{\Delta} (\mathbf{W}_{tm} \cdot \mathbf{W}_{tn}) ds \quad (132)$$

$$T_{\text{el}(tz)} = \frac{1}{\mu_r} \int_{\Delta} (\mathbf{W}_{tm} \cdot \nabla \alpha_j) ds \quad (133)$$

$$T_{\text{el}(zt)} = \frac{1}{\mu_r} \int_{\Delta} (\nabla \alpha_i \cdot \mathbf{W}_{tn}) ds \quad (134)$$

$$T_{\text{el}(zz)} = \frac{1}{\mu_r} \int_{\Delta} (\nabla \alpha_i \cdot \nabla \alpha_j) ds - k_o^2 \varepsilon_r \int_{\Delta} \alpha_i \alpha_j ds \quad (135)$$

These element matrices can be assembled over all the triangles in the cross section of the waveguide to obtain a global eigenvalue equation.

$$\begin{bmatrix} S_{tt} & 0 \\ 0 & 0 \end{bmatrix} \begin{bmatrix} e_t \\ e_z \end{bmatrix} = (-\beta^2) \begin{bmatrix} T_{tt} & T_{tz} \\ T_{zt} & T_{zz} \end{bmatrix} \begin{bmatrix} e_t \\ e_z \end{bmatrix} \quad (136)$$

2.2.4.4. Finite element matrices. Closed-form expressions are derived for the finite element matrices in equations (130) through (134). From equations (66) and (67),

$$S_{\text{el}(tt)} = \frac{1}{\mu_r} \left[\frac{L_{tm} L_{tn}}{16A^3} \left(D_m D_n - k_o^2 \varepsilon_r \sum_{k=1}^5 I_{tk} \right) \right] \quad (137)$$

With equations (73) through (77) and the procedures in sections 2.2.1 and 2.2.2, the remaining element matrices are derived as follows:

$$\begin{aligned} T_{\text{el}(tz)} &= \frac{1}{\mu_r} \frac{L_{tm}}{8A^2} [b_j (A_m + B_m \bar{y}_{\text{tri}}) \\ & + c_j (C_m + D_m \bar{x}_{\text{tri}})] \end{aligned} \quad (138)$$

$$\begin{aligned} T_{\text{el}(zt)} &= \frac{1}{\mu_r} \frac{L_{tn}}{8A^2} [b_i (A_n + B_n \bar{y}_{\text{tri}}) \\ & + c_i (C_n + D_n \bar{x}_{\text{tri}})] \end{aligned} \quad (139)$$

$$S_{\text{el}(zz)} = \frac{1}{\mu_r} \frac{b_i b_j + c_i c_j}{4A} \quad (140)$$

$$T_{\text{el}(tt)} = \varepsilon_r \frac{L_{tm} L_{tn}}{16A^3} \sum_{k=1}^5 I_{tk} \quad (141)$$

$$\left. \begin{aligned} T_{\text{el}(zz)} &= \frac{1}{\mu_r} \frac{b_i^2 + c_i^2}{4A} + k_o^2 \varepsilon_r \frac{A}{6} & (i = j) \\ &= \frac{1}{\mu_r} \frac{b_i b_j + c_i c_j}{4A} + k_o^2 \varepsilon_r \frac{A}{12} & (i \neq j) \end{aligned} \right\} \quad (142)$$

2.2.4.5. Numerical examples. A computer program HELMVEC3 was written to calculate the dispersion characteristics of inhomogeneously filled waveguides. For the first example for a partially filled rectangular waveguide with $b_r/a_r = 0.45$, $d/b_r = 0.5$, and $\varepsilon_r = 2.45$ shown in figure 12, the values of β/k_o are calculated and compared with analytical results given by Harrington (ref. 9, p. 161). The numerical results are presented in table 9 as a function of a_r/λ_o . The rectangular waveguide for this first example is modelled by 100 triangular elements.

Table 9. Dispersion Characteristics of Partially Filled Rectangular Waveguide of Figure 12

b_r/λ_o	β/k_o	
	Analytical (ref. 9)	HELMVEC3
0.2	0.48	0.47
0.3	1.00	1.01
0.4	1.18	1.17
0.5	1.26	1.28
0.6	1.30	1.35

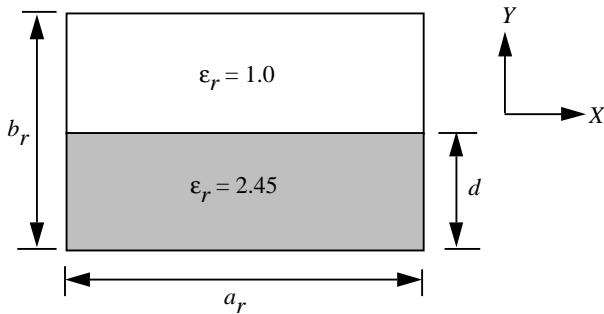


Figure 12. Partially filled rectangular waveguide with $b_r/a_r = 0.45$, $d/b_r = 0.5$, and $\varepsilon_r = 2.45$.

For the second example for a partially filled rectangular waveguide with $b_r/a_r = 0.45$ and $\varepsilon_r = 2.45$ shown in figure 13, the dispersion characteristics were also calculated and compared with those given by Harrington (ref. 9, p. 162). The numerical results are presented in table 10. The rectangular waveguide for this second example is also modelled by 100 triangular elements.

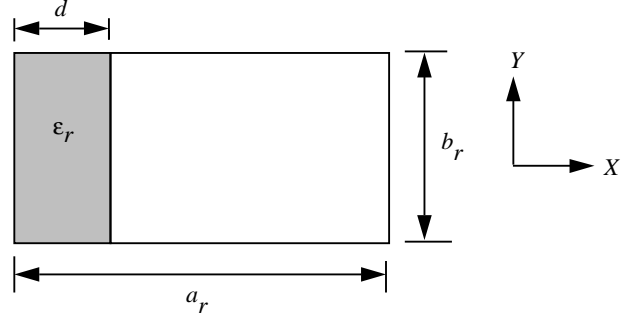


Figure 13. Partially filled waveguide with $b_r/a_r = 0.45$ and $\varepsilon_r = 2.45$.

2.2.5. Summary

In section 2.2, a detailed formulation for vector finite elements for two-dimensional eigenvalue problems in electromagnetics has been presented. Edge elements are used to impose divergence free condition on fields and hence the nonphysical modes (ref. 2), which plagued vector finite elements for many years are avoided. When assembling the global matrices from element matrices with edge basis functions, a unique global edge direction is defined to ensure field continuity across all edges. The basis function is multiplied by -1 , if the local edge vector does not have the same direction as the global edge direction. The numerical examples presented show the validity and accuracy of the analyses and computer codes, respectively. Both the formulation and the computer codes are valid for any arbitrarily shaped waveguides filled with inhomogeneous materials.

3. Three-Dimensional Problems

3.1. Eigenvalues of Three-Dimensional Cavity—Vector Formulation

The problem of calculating resonant frequencies of three-dimensional cavities has been plagued by spurious modes for many years. As mentioned in section 2.2, this problem has been recently overcome by using vector-based tangential edge elements (refs. 15 and 16). In section 3.1, we formulate the Galerkin finite element method for three-dimensional cavities and present results for various shapes of cavities.

Table 10. Dispersion Characteristics of Partially Filled Rectangular Waveguide of Figure 13

a_r/λ_o	β/k_o	
	Analytical (ref. 9)	HELMVEC3
$d/a_r = 0$		
0.4		
0.5	0.03	0.04
0.6	0.52	0.56
0.7	0.70	0.71
0.8	0.79	0.78
0.9	0.83	0.83
1.0	0.88	0.87
$d/a_r = 0.167$		
0.4		
0.5	0.21	0.18
0.6	0.60	0.59
0.7	0.72	0.74
0.8	0.82	0.81
0.9	0.88	0.87
1.0	0.91	0.90
$d/a_r = 0.286$		
0.4		
0.5	0.51	0.44
0.6	0.78	0.74
0.7	0.90	0.88
0.8	0.99	1.05
0.9	1.03	1.03
1.0	1.10	1.09
$d/a_r = 0.375$		
0.4		
0.5	0.68	0.66
0.6	0.91	0.90
0.7	1.05	1.03
0.8	1.13	1.11
0.9	1.20	1.18
1.0	1.25	1.23
$d/a_r = 0.5$		
0.4	0.40	0.42
0.5	0.90	0.89
0.6	1.10	1.09
0.7	1.20	1.19
0.8	1.25	1.24
0.9	1.30	1.31
1.0	1.35	1.35
$d/a_r = 0.6$		
0.4	0.70	0.67
0.5	1.02	1.03
0.6	1.18	1.19
0.7	1.23	1.27
0.8	1.31	1.33
0.9	1.38	1.37
1.0	1.41	1.40
$d/a_r = 0.8$		
0.4	0.90	0.91
0.5	1.18	1.18
0.6	1.29	1.30
0.7	1.38	1.37
0.8	1.41	1.42
0.9	1.43	1.44
1.0	1.44	1.47

3.1.1. Formulation

This formulation can be followed by using either the \mathbf{E} or \mathbf{H} field. We illustrate the \mathbf{E} field formulation. Consider the vector wave equation,

$$\nabla \times \left(\frac{1}{\mu_r} \nabla \times \mathbf{E} \right) - k_o^2 \varepsilon_r \mathbf{E} = 0 \quad (143)$$

where

$$\mathbf{E} = E_x \hat{x} + E_y \hat{y} + E_z \hat{z}$$

Introduce a testing function $\mathbf{T} = T_x \hat{x} + T_y \hat{y} + T_z \hat{z}$. To apply Galerkin's method, multiply equation (143) with \mathbf{T} and integrate over the volume of the cavity v :

$$\iiint_v \left(\mathbf{T} \cdot \nabla \times \left(\frac{1}{\mu_r} \nabla \times \mathbf{E} \right) - k_o^2 \varepsilon_r \mathbf{T} \cdot \mathbf{E} \right) dv = 0 \quad (144)$$

With the vector identity,

$$\mathbf{A} \cdot (\nabla \times \mathbf{B}) = (\nabla \times \mathbf{A}) \cdot \mathbf{B} - \nabla \cdot (\mathbf{A} \times \mathbf{B}) \quad (145)$$

equation (144) can be written as

$$\begin{aligned} \iiint_v (\nabla \times \mathbf{T}) \cdot \left(\frac{1}{\mu_r} \nabla \times \mathbf{E} \right) dv &= k_o^2 \varepsilon_r \iiint_v \mathbf{T} \cdot \mathbf{E} ds \\ &+ \iiint_v \nabla \cdot \left[\mathbf{T} \times \left(\frac{1}{\mu_r} \nabla \times \mathbf{E} \right) \right] dv \end{aligned} \quad (146)$$

Invoking the divergence theorem

$$\iiint_v \nabla \cdot \mathbf{A} dv = \iint_S \mathbf{A} \cdot \hat{n} ds \quad (147)$$

and

$$(\mathbf{A} \times \mathbf{B}) \cdot \hat{n} = -\mathbf{A} \cdot (\hat{n} \times \mathbf{B}) \quad (148)$$

where v indicates the integration over the volume of the cavity, S indicates the integration over the outer surface of the cavity, and \hat{n} is the outward unit vector normal to the surface, equation (146) becomes

$$\begin{aligned} \iiint_v (\nabla \times \mathbf{T}) \cdot \left(\frac{1}{\mu_r} \nabla \times \mathbf{E} \right) dv &= k_o^2 \varepsilon_r \iiint_v \mathbf{T} \cdot \mathbf{E} dv \\ &- \iint_S \mathbf{T} \cdot \left[\hat{n} \times \left(\frac{1}{\mu_r} \nabla \times \mathbf{E} \right) \right] ds \end{aligned} \quad (149)$$

For a cavity bounded by perfectly conducting electric conductor, the field as well as the testing function \mathbf{T} has to be zero on the outer surface; hence,

the last term on the right-hand side of equation (149) vanishes. Equation (149) can be written in its final form as

$$\iiint_v (\nabla \times \mathbf{T}) \cdot \left(\frac{1}{\mu_r} \nabla \times \mathbf{E} \right) dv = k_o^2 \varepsilon_r \iiint_v \mathbf{T} \cdot \mathbf{E} dv \quad (150)$$

3.1.2. Discretization

The volume of the cavity is discretized by using first-order tetrahedral elements such as the one shown in figure 14. The first-order tetrahedron has four nodes and six edges. The six edges are formed as shown in table 11.

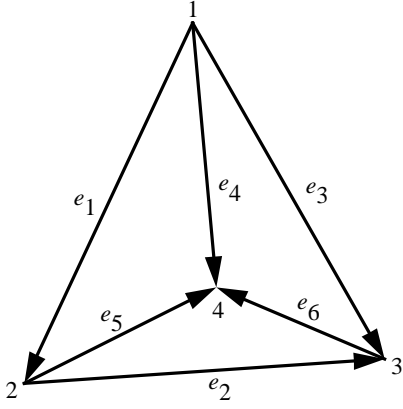


Figure 14. First-order tetrahedral element.

Table 11. Formation of Edges of Tetrahedral Element

Edge, m	Node	
	i	j
1	1	2
2	2	3
3	1	3
4	1	4
5	2	4
6	3	4

The electric field in a single tetrahedral element is represented as

$$\mathbf{E} = \sum_{m=1}^6 e_m \mathbf{W}_m \quad (151)$$

The six unknown parameters associated with each edge are e_1, e_2, \dots, e_6 . The total field is obtained by evaluating equation (151).

The vector tangential edge elements \mathbf{W}_m are given by (ref. 3)

$$\mathbf{W}_m = L_m (\alpha_{ti} \nabla \alpha_{tj} - \alpha_{tj} \nabla \alpha_{ti}) \quad (152)$$

In equation (152), m stands for edge number, i and j stand for the nodes connecting edge i , L_m is the length of the edge m , α_{ti} and α_{tj} are the simplex coordinates associated with nodes i and j .

The simplex coordinates for the nodes of a tetrahedron element are given by Silvester and Ferrari in reference 1

$$\alpha_{t1} = \frac{V_1}{V} \quad (153)$$

$$\alpha_{t2} = \frac{V_2}{V} \quad (154)$$

$$\alpha_{t3} = \frac{V_3}{V} \quad (155)$$

$$\alpha_{t4} = \frac{V_4}{V} \quad (156)$$

where V is the volume of the tetrahedron given by

$$V = \frac{1}{6} \begin{vmatrix} 1 & x_1 & y_1 & z_1 \\ 1 & x_2 & y_2 & z_2 \\ 1 & x_3 & y_3 & z_3 \\ 1 & x_4 & y_4 & z_4 \end{vmatrix} \quad (157)$$

$$V_1 = \frac{1}{6} \begin{vmatrix} 1 & x & y & z \\ 1 & x_2 & y_2 & z_2 \\ 1 & x_3 & y_3 & z_3 \\ 1 & x_4 & y_4 & z_4 \end{vmatrix} \quad (158)$$

$$V_2 = \frac{1}{6} \begin{vmatrix} 1 & x_1 & y_1 & z_1 \\ 1 & x & y & z \\ 1 & x_3 & y_3 & z_3 \\ 1 & x_4 & y_4 & z_4 \end{vmatrix} \quad (159)$$

$$V_3 = \frac{1}{6} \begin{vmatrix} 1 & x_1 & y_1 & z_1 \\ 1 & x_2 & y_2 & z_2 \\ 1 & x & y & z \\ 1 & x_4 & y_4 & z_4 \end{vmatrix} \quad (160)$$

$$V_4 = \frac{1}{6} \begin{vmatrix} 1 & x_1 & y_1 & z_1 \\ 1 & x_2 & y_2 & z_2 \\ 1 & x_3 & y_3 & z_3 \\ 1 & x & y & z \end{vmatrix} \quad (161)$$

For any node ($i = 1, 2, 3, 4$), α_{ti} is given by

$$\alpha_{ti} = \frac{a_{ti} + b_{ti}x + c_{ti}y + d_{ti}z}{6V} \quad (162)$$

where a_{ti} , b_{ti} , c_{ti} , and d_{ti} are appropriate cofactors picked from the determinants in V_1 , V_2 , V_3 , and V_4 for $m = 1, 2, 3$, and 4 , respectively. From equations (152) and (162), the edge elements are given as

$$\begin{aligned}\mathbf{W}_m = & \frac{L_m}{36V^2}[(A_{xm} + B_{xm}y + C_{xm}z)\hat{x} \\ & + (A_{ym} + B_{ym}x + C_{ym}z)\hat{y} \\ & + (A_{zm} + B_{zm}x + C_{zm}y)\hat{z}] \quad (163)\end{aligned}$$

where

$$A_{xm} = a_{ti}b_{tj} - a_{tj}b_{ti} \quad (164)$$

$$B_{xm} = c_{ti}b_{tj} - c_{tj}b_{ti} \quad (165)$$

$$C_{xm} = d_{ti}b_{tj} - d_{tj}b_{ti} \quad (166)$$

$$A_{ym} = a_{ti}c_{tj} - a_{tj}c_{ti} \quad (167)$$

$$B_{ym} = b_{ti}c_{tj} - b_{tj}c_{ti} = -B_{xm} \quad (168)$$

$$C_{ym} = d_{ti}c_{tj} - d_{tj}c_{ti} \quad (169)$$

$$A_{zm} = a_{ti}d_{tj} - a_{tj}d_{ti} \quad (170)$$

$$B_{zm} = b_{ti}d_{tj} - b_{tj}d_{ti} = -C_{xm} \quad (171)$$

$$C_{zm} = c_{ti}d_{tj} - c_{tj}d_{ti} = -C_{ym} \quad (172)$$

Also \mathbf{W}_m can be shown to satisfy the condition,

$$\hat{t}_m \cdot \mathbf{W}_m = \begin{cases} 1 & (\text{edge } m) \\ 0 & (\text{other edges}) \end{cases} \quad (173)$$

where \hat{t}_m is the unit vector along the direction of the edge.

3.1.3. Finite Element Formulation

Substituting equation (151) into equation (150), integrating over the volume of one tetrahedral element, and interchanging the summation and integration give

$$\begin{aligned}& \frac{1}{\mu_r} \sum_{m=1}^6 \int \int \int_{\blacktriangle} (\nabla \times \mathbf{W}_m) \cdot (\nabla \times \mathbf{W}_n) e_m dv \\ & = k_o^2 \sum_{m=1}^6 \varepsilon_r \int \int \int_{\blacktriangle} (\mathbf{W}_m \cdot \mathbf{W}_n) e_m dv \\ & (n = 1, 2, \dots, 6) \quad (174)\end{aligned}$$

where \blacktriangle indicates integration over the volume of tetrahedron. This can be written in matrix form as

$$[S_{el}][e] = k_o^2 [T_{el}][e] \quad (175)$$

where the element matrices are given by

$$[S_{el}] = \frac{1}{\mu_r} \int \int \int_{\blacktriangle} (\nabla \times \mathbf{W}_m) \cdot (\nabla \times \mathbf{W}_n) dv \quad (176)$$

$$[T_{el}] = \varepsilon_r \int \int \int_{\blacktriangle} (\mathbf{W}_m \cdot \mathbf{W}_n) dv \quad (177)$$

These element matrices can be assembled over all the tetrahedral elements in the cavity volume to obtain a global eigenmatrix equation,

$$[\mathbf{S}][e] = k_o^2 [\mathbf{T}][e] \quad (178)$$

To ensure field continuity across all edges, a unique global edge direction is defined (i.e., always pointing from the smaller node number to the larger node number) so that equation (151) has to be multiplied by -1 , if the local edge vector does not have the same direction as the global edge direction.

The electric field is zero on the PEC boundaries. It is imposed by taking the coefficients of equation (151) as zeros. In other words, the edges on the boundary are simply ignored when forming the finite element matrices and hence reducing the order of the matrices to be solved.

3.1.4. Finite Element Matrices

The aim of this section is to obtain closed-form expressions for equations (176) and (177). From equation (163),

$$\nabla \times \mathbf{W}_m = \frac{L_m}{18V^2} (C_{zm}\hat{x} + C_{xm}\hat{y} + B_{ym}\hat{z}) \quad (179)$$

and hence

$$\begin{aligned}(\nabla \times \mathbf{W}_m) \cdot (\nabla \times \mathbf{W}_n) &= \frac{L_m L_n}{(18V^2)^2} \\ &\times (C_{zm}C_{zn} + C_{xm}C_{xn} + B_{ym}B_{yn}) \quad (180)\end{aligned}$$

From equations (176), (177), and (180), and making use of the integration formulas given in reference 18, the closed-form expressions for element matrices are given as

$$S_{el} = \frac{L_m L_n}{324V^3 \mu_r} (C_{zm}C_{zn} + C_{xm}C_{xn} + B_{ym}B_{yn}) \quad (181)$$

$$T_{el} = \varepsilon_r \frac{L_m L_n}{1296V^3} \sum_{k=1}^{10} I_k \quad (182)$$

where

$$\begin{aligned}
I_1 &= A_{xm}A_{xn} + A_{ym}A_{yn} + A_{zm}A_{zn} \\
I_2 &= (A_{ym}B_{yn} + A_{yn}B_{ym} + A_{zm}B_{zn} + A_{zn}B_{zm})\bar{x}_{\text{tet}} \\
I_3 &= (A_{xm}B_{xn} + A_{xn}B_{xm} + A_{zm}C_{zn} + A_{zn}C_{zm})\bar{y}_{\text{tet}} \\
I_4 &= (A_{xm}C_{xn} + A_{xn}C_{xm} + A_{ym}C_{yn} + A_{yn}C_{ym})\bar{z}_{\text{tet}} \\
I_5 &= \frac{1}{20}(B_{zm}C_{zn} + B_{zn}C_{zm})\left(\sum_{i=1}^4 x_i y_i + 16\bar{x}_{\text{tet}}\bar{y}_{\text{tet}}\right) \\
I_6 &= \frac{1}{20}(B_{xm}C_{xn} + B_{xn}C_{xm})\left(\sum_{i=1}^4 y_i z_i + 16\bar{y}_{\text{tet}}\bar{z}_{\text{tet}}\right) \\
I_7 &= \frac{1}{20}(B_{ym}C_{yn} + B_{yn}C_{ym})\left(\sum_{i=1}^4 x_i z_i + 16\bar{x}_{\text{tet}}\bar{z}_{\text{tet}}\right) \\
I_8 &= \frac{1}{20}(B_{ym}B_{yn} + B_{zm}B_{zn})\left(\sum_{i=1}^4 x_i^2 + 16\bar{x}_{\text{tet}}^2\right) \\
I_9 &= \frac{1}{20}(B_{xm}B_{xn} + C_{zm}C_{zn})\left(\sum_{i=1}^4 y_i^2 + 16\bar{y}_{\text{tet}}^2\right) \\
I_{10} &= \frac{1}{20}(C_{xm}C_{xn} + C_{ym}C_{yn})\left(\sum_{i=1}^4 z_i^2 + 16\bar{z}_{\text{tet}}^2\right)
\end{aligned}$$

3.1.5. Numerical Examples

A computer program FEM3D0 was written to calculate the eigenvalues of a three-dimensional cavity. For a three-dimensional problem, the number of variables increases drastically compared with those for a two-dimensional problem. Hence it is not economical to use a generalized eigenvalue solver. The program FEM3D1 was written to take advantage of the sparse nature of the finite element matrices. This program exploits the symmetry of the matrices and stores only the nonzero entries in the lower triangle of the matrices; hence, considerable savings in memory result. It also makes use of the sparse eigenvalue solvers available in VECLIB (ref. 19) and results in faster computation.

The following numerical examples have been taken from Chatterjee, Jin, and Volakis (ref. 17), in which the resonant wave numbers for various three-dimensional cavities have been calculated by using a different kind of edge elements. The analytical results mentioned here are also taken from reference 17.

Air-filled rectangular cavity: The eigenvalues of an air-filled rectangular cavity (shown in fig. 15)

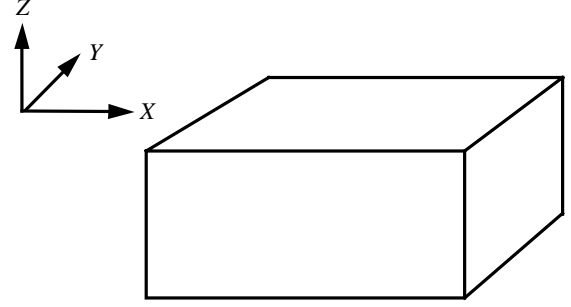


Figure 15. Air-filled rectangular cavity. Size: 1 by 0.5 by 0.75 cm.

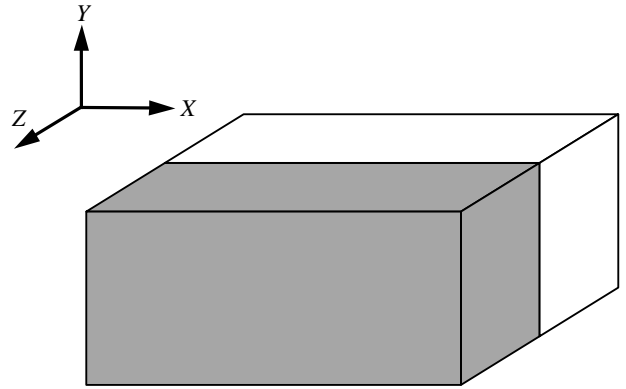


Figure 16. Half-filled rectangular cavity with dielectric material $\epsilon_r = 2.0$ and filled from $z = 0.5$ to 1 cm. Size: 1 by 0.1 by 1 cm.

were calculated by FEM3D1 and are presented in table 12. The cavity geometry is represented by 343 tetrahedral elements.

Table 12. Eigenvalues of Air-Filled Rectangular Cavity

Mode	k_o, cm^{-1}		
	Analytical (ref. 17)	FEM3D1 (343 elements)	Reference 17
TE ₁₀₁	5.236	5.242	5.213
TM ₁₁₀	7.025	6.942	6.977
TE ₀₁₁	7.531	7.372	7.474
TE ₂₀₁	7.531	7.560	7.573
TE ₁₁₁	8.179	8.064	7.991
TM ₁₁₁	8.179	8.164	8.122
TM ₂₁₀	8.886	8.725	8.572
TE ₁₀₂	8.947	8.871	8.795

Half-filled rectangular cavity: A half-filled (filled from $z = 0.5$ to 1 cm) rectangular cavity with dielectric material $\epsilon_r = 2.0$ is shown in figure 16.

The eigenvalues were calculated by FEM3D1 and are presented in table 13. The cavity geometry was modelled with 615 tetrahedral elements.

Table 13. Eigenvalues of Half-Filled Rectangular Cavity

Mode	k_o, cm^{-1}		
	Analytical	FEM3D1 (615 elements)	Reference 17
TE_{z101}	3.538	3.524	3.534
TE_{z201}	5.445	5.401	5.440
TE_{z102}	5.935	5.931	5.916
TE_{z301}	7.503	7.382	7.501
TE_{z202}	7.633	7.562	7.560
TE_{z103}	8.096	8.003	8.056

Circular cylindrical cavity: The eigenvalues of an air-filled circular cylindrical cavity (shown in fig. 17) were calculated by FEM3D1 and are presented in table 14. The geometry of this cavity was represented by 633 tetrahedral elements.

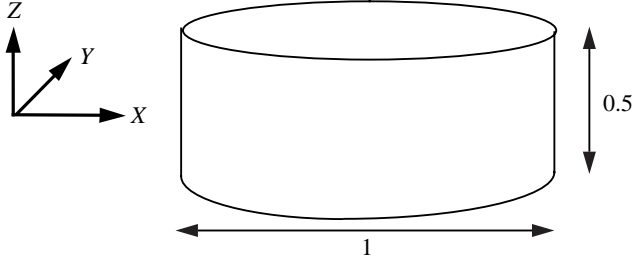


Figure 17. Air-filled circular cylindrical cavity. Dimensions are in centimeters.

Table 14. Eigenvalues of Air-Filled Circular Cylindrical Cavity

Mode	k_o, cm^{-1}		
	Analytical	FEM3D1 (633 elements)	Reference 17
TM_{010}	4.810	4.782	4.809
TE_{111}	7.283	7.210	7.202
TE_{111}	7.283	7.290	7.288
TM_{110}	7.650	7.575	7.633
TM_{110}	7.650	7.620	7.724
TM_{011}	7.840	7.901	7.940
TE_{211}	8.658	8.676	8.697
TE_{211}	8.658		8.865

Spherical cavity: The spherical cavity geometry was represented by 473 tetrahedral elements. The

eigenvalues, calculated by FEM3D1, are presented in table 15. The spherical cavity had a radius of 1 cm.

Table 15. Eigenvalues of Spherical Cavity With Radius of 1 cm

Mode	k_o, cm^{-1}		
	Analytical	FEM3D1 (473 elements)	Reference 16
TM_{010}	2.744	2.799	2.799
TM_{010}	2.744	2.802	2.802
TM_{010}	2.744	2.807	2.811
TM_{021}	3.870	3.961	3.948
TM_{121} , even	3.870	3.976	3.986
TM_{121} , odd	3.870	3.986	3.994
TM_{221} , even	3.870	3.994	4.038
TM_{221} , odd	3.870	3.998	4.048
TE_{011}	4.493	4.421	4.433
TE_{111} , even	4.493	4.478	4.472
TE_{111} , odd	4.493	4.501	4.549

3.1.6. Summary

In section 3.1, vector finite elements introduced in section 2.2 are extended to solve three-dimensional eigenvalue problems by using tangential edge basis functions for tetrahedral elements. Spurious solutions are completely avoided because of the divergence free nature of the edge elements. Sparse matrix eigenvalue solvers are used to take advantage of the sparsity and symmetry of the finite element matrices; this results in considerable savings in computer memory and computational time. The numerical results presented for cavities with different shapes prove the validity of the analysis and accuracy of the computer codes presented in this section.

4. Concluding Remarks

A thorough formulation of FEM for various eigenvalue problems in electromagnetism has been presented. The use of recently developed edge basis functions for vector finite elements has been demonstrated for two-dimensional and three-dimensional problems. Triangular elements for two-dimensional problems and tetrahedral elements for three-dimensional problems are used to model complex geometrical shapes because of their ability to represent such shapes accurately.

Implementation of conventional nodal-based scalar formulation for two-dimensional homogeneous problems is demonstrated in section 2.1. The computer code developed can be used to calculate the

eigenvalues and field intensity patterns of any arbitrarily shaped waveguide filled with homogeneous material. The numerical results for various waveguides and the field intensity patterns for various modes have been presented in section 2.1 which show the validity of the analysis and computer code. Simple waveguide shapes have been chosen for demonstration purposes because their field distributions are well known.

In section 2.2, the two-dimensional edge basis functions for triangular elements are introduced to model transverse vector fields in waveguides. For waveguides or microwave circuit design problems in general, knowledge of a propagation constant at a given frequency is desirable. A step-by-step formulation is done to determine either the wave number or the propagation constant, if one of them is specified. Numerical examples are presented to validate the analysis and the computer codes.

Since real problems involve three-dimensional geometries, a formulation for the calculation of eigen-

values for such geometries is presented in section 3. The three-dimensional edge basis functions are introduced for tetrahedral elements. Numerical examples for various geometries are presented. Comparison of the numerical data with the available data in the literature shows the validity and accuracy of the analysis.

For the three-dimensional problems, the number of variables increases drastically compared with those for the two-dimensional problems. In the three-dimensional computer codes, sparsity of FEM matrices have been exploited by storing only the nonzero elements and symmetry is utilized by storing only either the upper or lower part of the matrices. The sparse matrix eigenvalue solvers are used to efficiently solve the FEM equations.

NASA Langley Research Center
Hampton, VA 23681-0001
October 3, 1994

Appendix

Computer Programs

Computer programs were written to implement the analysis presented in this report. All the programs are written in FORTRAN language. These programs take *.MOD file containing the meshing information from COSMOS/M (ref. 4). Also these computer programs make use of the optimized library routines of EISPACK (refs. 7 and 8) and VECLIB (ref. 18) on the CONVEX computer.

HELM10 is a two-dimensional finite element program to calculate the eigenvalues of homogeneously filled waveguides. This program implements the analysis described in section 2.1.

HELMVEC is a two-dimensional finite element program to calculate the eigenvalues of homogeneously filled waveguides. Unlike HELM10, this program uses the vector basis functions and implements the analysis presented in section 2.2.1.

HELMVEC1 is a two-dimensional finite element program to calculate the eigenvalues of inhomogeneously filled waveguides. This program implements the three-component vector field formulation discussed in section 2.2.2 and makes use of edge basis functions for transverse fields and scalar basis functions associated with nodes for longitudinal fields.

HELMVEC2 is a two-dimensional finite element program for finding out the wave number of an inhomogeneously filled waveguide when the propagation constant is specified. This program implements the formulation presented in section 2.2.3.

HELMVEC3 is a two-dimensional finite element program for determination of propagation constant of an inhomogeneously filled waveguide at any frequency. This program implements the formulation given in section 2.2.4.

FEM3D0 and FEM3D1 are three-dimensional finite element programs to calculate the eigenvalues of inhomogeneously filled cavities. These programs implement the formulation presented in section 3.1. FEM3D0 uses the EISPACK (refs. 7 and 8) routines, whereas FEM3D1 exploits the sparsity and symmetry of FEM matrices and uses VECLIB (ref. 19) routines.

These computer programs are available on request from

Information and Electromagnetic Technology
Division
Electromagnetic Research Branch
M.S. 490
NASA Langley Research Center
Hampton VA 23681-0001

References

1. Silvester, P. P.; and Ferrari, R. L.: *Finite Elements for Electrical Engineers*. Second ed., Cambridge Univ. Press, 1990.
2. Rahman, B. M. Azizur; and Davies, J. Brian: Penalty Function Improvement of Waveguide Solution by Finite Elements. *IEEE Trans. Microw. Theory & Techni.*, vol. MTT-32, no. 8, Aug. 1984, pp. 922–928.
3. Bossavit, Alain: Simplicial Finite Elements for Scattering Problems in Electromagnetism. *Comput. Methods Appl. Mech. & Eng.*, vol. 76, 1989, pp. 299–316.
4. *COSMOS/M—User Guide*. Volume 1—Preprocessing, Analysis and Postprocessing Interface, Version 1.70. Structural Research and Analysis Corp., May 1993.
5. *I-DEAS Relational Data Base*. I-DEAS V Prod. Bul., Structural Dynamics Research Corp., Jan. 1990.
6. Silvester, P.: Construction of Triangular Finite Element Universal Matrices. *Int. J. Numer. Methods Eng.* vol. 12, no. 2, 1978, pp. 237–244.
7. Smith, B. T.; Boyle, J. M.; Dongarra, J. J.; Garbow, B. S.; Ikebe, Y.; Klema, V. C.; and Moler, C. B.: *Matrix Eigensystem Routines—EISPACK Guide*. Second Ed., Springer-Verlag, 1976.
8. Garbow, B. S.; Boyle, J. M.; Dongarra, J. J.; and Moler, C. B.: *Matrix Eigensystem Routines—EISPACK Guide Extension*. Springer-Verlag, 1977.
9. Harrington, Roger F.: *Time-Harmonic Electromagnetic Fields*. McGraw-Hill Book Co., Inc., 1961.
10. Marcuvitz, N., ed.: *Waveguide Handbook*. McGraw-Hill Book Co., Inc., 1951.
11. Koshiba, Masanori; Hayata, Kazuya; and Suzuki, Michio: Improved Finite-Element Formulation in Terms of the Magnetic Field Vector for Dielectric Waveguides. *IEEE Trans. Microw. Theory & Techni.*, vol. MTT-33, no. 3, Mar. 1985, pp. 227–233.
12. Whitney, Hassler: *Geometric Integration Theory*. Princeton Univ. Press, 1957.
13. Lee, J.-F.; Sun, D. K.; and Cendes, Z. J.: Full-Wave Analysis of Dielectric Waveguides Using Tangential Vector Finite Elements. *IEEE Trans. Microw. Theory & Techni.*, vol. 39, no. 8, Aug. 1991, pp. 1262–1271.
14. Reddy, J. N.: *An Introduction to the Finite Element Method*. McGraw-Hill Book Co., Inc., 1984.
15. Hayata, Kazuya; Koshiba, Masanori; Eguchi, Masashi; and Suzuki, Michio: Vectorial Finite-Element Method Without Any Spurious Solutions for Dielectric Waveguiding Problems Using Transverse Magnetic-Field Component. *IEEE Trans. Microw. Theory & Techni.*, vol. MTT-34, no. 11, Nov. 1986, pp. 1120–1124.
16. Lee, Jin-Fa; and Mittra, Raj: A Note on the Application of Edge-Elements for Modeling Three-Dimensional Inhomogeneously-Filled Cavities. *IEEE Trans. Microw. Theory & Techni.*, vol. 40, no. 9, Sept. 1992, pp. 1767–1773.
17. Chatterjee, A.; Jin, J. M.; and Volakis, J. L.: Computation of Cavity Resonances Using Edge-Based Finite Elements. *IEEE Trans. Microw. Theory & Techni.*, vol. 40, no. 11, Nov. 1992, pp. 2106–2108.
18. Zienkiewicz, O. C.: *The Finite Element Method in Engineering Science*. McGraw-Hill Book Co., Inc., 1971.
19. *CONVEX VECLIB—User's Guide*, Seventh ed., CONVEX Computer Corp., 1993.

REPORT DOCUMENTATION PAGE			Form Approved OMB No. 0704-0188	
Public reporting burden for this collection of information is estimated to average 1 hour per response, including the time for reviewing instructions, searching existing data sources, gathering and maintaining the data needed, and completing and reviewing the collection of information. Send comments regarding this burden estimate or any other aspect of this collection of information, including suggestions for reducing this burden, to Washington Headquarters Services, Directorate for Information Operations and Reports, 1215 Jefferson Davis Highway, Suite 1204, Arlington, VA 22202-4302, and to the Office of Management and Budget, Paperwork Reduction Project (0704-0188), Washington, DC 20503.				
1. AGENCY USE ONLY (Leave blank)		2. REPORT DATE December 1994	3. REPORT TYPE AND DATES COVERED Technical Paper	
4. TITLE AND SUBTITLE Finite Element Method for Eigenvalue Problems in Electromagnetics			5. FUNDING NUMBERS WU 505-64-52-04	
6. AUTHOR(S) C. J. Reddy, Manohar D. Deshpande, C. R. Cockrell, and Fred B. Beck				
7. PERFORMING ORGANIZATION NAME(S) AND ADDRESS(ES) NASA Langley Research Center Hampton, VA 23681-0001			8. PERFORMING ORGANIZATION REPORT NUMBER L-17392	
9. SPONSORING/MONITORING AGENCY NAME(S) AND ADDRESS(ES) National Aeronautics and Space Administration Washington, DC 20546-0001			10. SPONSORING/MONITORING AGENCY REPORT NUMBER NASA TP-3485	
11. SUPPLEMENTARY NOTES Reddy: NRC-NASA Resident Research Associate, Langley Research Center, Hampton, VA; Deshpande: ViGYAN, Inc., Hampton, VA; Cockrell and Beck: Langley Research Center, Hampton, VA.				
12a. DISTRIBUTION/AVAILABILITY STATEMENT Unclassified-Unlimited Subject Category 32 Availability: NASA CASI (301) 621-0390			12b. DISTRIBUTION CODE	
13. ABSTRACT (Maximum 200 words) Finite element method (FEM) has been a very powerful tool to solve many complex problems in electromagnetics. The goal of the current research at the Langley Research Center is to develop a combined FEM/method of moments approach to three-dimensional scattering/radiation problem for objects with arbitrary shape and filled with complex materials. As a first step toward that goal, an exercise is taken to establish the power of FEM, through closed boundary problems. This paper demonstrates the development of FEM tools for two- and three-dimensional eigenvalue problems in electromagnetics. In section 2, both the scalar and vector finite elements have been used for various waveguide problems to demonstrate the flexibility of FEM. In section 3, vector finite element method has been extended to three-dimensional eigenvalue problems.				
14. SUBJECT TERMS Finite element; Waveguide; Eigenvalues; Computational method; Electromagnetic			15. NUMBER OF PAGES 36	
			16. PRICE CODE A03	
17. SECURITY CLASSIFICATION OF REPORT Unclassified	18. SECURITY CLASSIFICATION OF THIS PAGE Unclassified	19. SECURITY CLASSIFICATION OF ABSTRACT Unclassified	20. LIMITATION OF ABSTRACT	